Chapter 6

Intermediate mass region analysis

In this chapter, after a detailed introduction, the pA, SU and PbPb dimuon mass spectra are analysed. The intermediate mass spectrum is described as a superposition of DY and open charm (also indicated as $D\overline{D}$), after combinatorial background subtraction. The DY and $D\overline{D}$ contributions are extracted from the fit of the mass spectra. Since the DY contribution in the IMR is determined by the high mass region above the ψ', and since the background normalisation is fixed $a-priori$ using the R_{BCK} calculated in chapter 5, it is the $D\overline{D}$ contribution which will change accordingly with the experimental dimuon yield in the IMR.

For each system the $D\overline{D}/DY$ ratios are then derived. Since both the DY process and the $D\overline{D}$ hadro-production are hard processes and are therefore expected to scale with the number of effective nucleon-nucleon collisions in a nucleus-nucleus interaction (see chapter 1), any anomalous behaviour of the $D\overline{D}$ contribution will clearly show in the $D\overline{D}/DY$ ratio.

The pA systems, where no excess has been measured, are also analysed. The extracted $D\overline{D}/DY$ can then be used as a reference when calculating the absolute value of the excess for the SU and PbPb systems.

To support the results obtained with the analysis of the mass distributions, the dimuon p_T, y and $cos\theta$ distributions are also studied.

6.1 Introduction

In the present chapter, which with chapter 5 and 7 constitutes the core of my work, the analysis of the mass, p_T, rapidity and cosθ spectra of the SU, PbPb and pA systems is described. The different aspects of the analysis are dealt with in the following order :

- In sec.6.2, the general method used to fit the mass spectra is discussed. The aim of the fit of the mass spectra is the extraction of the $D\overline{D}$ contribution to the IMR region. The contribution to the IMR of all the other components are therefore established in some independent way. For instance, the DY contribution in the IMR is determined by the high mass region for M>4.5 GeV/c^2, where only DY events can be found. Moreover, the background contribution in the IMR mass spectra is fixed with the R_{BCK} factors calculated in chapter 5.

  It is perhaps important to stress that, since the combinatorial background contribution in the IMR amounts up to 85% in central S-U and in p-A collisions and up to 95% in central Pb-Pb collisions, the determination of the combinatorial background contribution to the IMR is one of the most important issues of the present analysis. In chapter 5, which has been completely devoted to the discussion of the combinatorial background, the so called R_{BCK} factor has been introduced. The R_{BCK} factor corrects the normalisation of the opposite-sign background when the multiplicity of secondaries produced in the collision (pions and kaons) is not large enough to motivate the assumption of a complete charge UN-correlation between the same produced secondaries. The R_{BCK} factor is expected to be larger than 1 in peripheral nucleus-nucleus collisions and in proton-nucleus ones, whereas it should be compatible with 1.0 in central nucleus-nucleus collisions. Chapter 5 gives a detailed description of the Monte-Carlo chain used to determine the R_{BCK} values for all the considered systems and for all the used E_T bins within the same system.

- Once the fit has been performed, the $D\overline{D}$ can be extracted and normalised to the corresponding DY contribution. In sec.6.3, the method used to obtain the ratio $D\overline{D}/DY$ is outlined.

  The DY contribution is used as a reference because it has been experimentally proved that the DY does behave as hard processes are expected to, i.e., the cross section for DY pair production in proton-nucleus and nucleus-nucleus interactions scales with the total number of effective nucleon-nucleon collisions (see chapter 1). The open charm hadro production is also a hard process and is therefore expected to behave as the DY does. This has been proved in proton-nucleus collisions, but up until now no direct measurement of open charm production in nucleus-nucleus collision has been performed. In nucleus-nucleus collisions charm production could also proceed through some alternative processes (see chapter 7 and references therein). Thereafter, if the $D\overline{D}/DY$ presents any anomalous behaviour, this can be associated with the intervention of a new contribution to the open charm component.

- Section 6.4 and 6.5 present the results of the analysis of the PbPb and SU mass differential distributions, which are then gathered and discussed in sec.6.6.

- In section 6.7, the p_T, y and cosθ differential distributions are studied.

When in sec. 6.4, 6.5 and 6.6 the mass differential distributions of the SU and PbPb systems are studied, the extracted $D\overline{D}/DY$ is found to increase with the size of the system and with the collision centrality. In order to support the hypothesis that the found excess in the IMR can be interpreted as an enhanced open charm production, the p_T, y and cosθ differential distributions can be studied. The p_T, y and cosθ Monte-Carlo differential distributions are normalised from the results of the fit of the mass spectra. The normalised Monte-Carlo distributions are then superimposed on the experimental ones. No additional hypothesis are introduced. In the p_T spectra the shapes of the DY and open charm contributions can be well distinguished, whereas in the y and cosθ ones the different contributions are all similar in shape. Thereafter, the p_T spectra are studied in detail.

- In sec.6.8, the pA systems are analysed in two slightly different ways and the pA reference value is given as a weighted average of the two extracted $D\overline{D}/DY$ values. In the same section, the pA p_T, y and $cos\theta$ differential distributions are also studied.

- In the last section, the results obtained in the present analysis are compared with the results which would have been obtained if the R_{BCK} values would have been set to 1.0 for all the E_T bins of the two considered nucleus-nucleus systems. This approach has been widely used in the past by the NA38/NA50 Collaboration and it is therefore important to be aware of the approximations induced by such an assumption.

Next, the effect of leaving the R_{BCK} factor as a free parameter in the fit is studied. This approach being generally wrong, it is still interesting to see if and when the shape of the experimental mass distribution alone is able to give a satisfactory estimation of the combinatorial background contribution.

The systematic error associated with the method used for the combinatorial background subtraction is also estimated.

6.2 Fit of the mass spectra : general method.

The fit of the opposite-sign experimental mass spectrum is performed using the Monte-Carlo fitting functions for all the participating processes. The following function is therefore constructed,

$$\frac{dN^{+-}}{dM} = R_{BCK}\frac{dN^{bck}}{dM} + n_{D\overline{D}}\frac{dN^{D\overline{D}}}{dM} + n_{DY}\frac{dN^{DY}}{dM} + n_{J/\psi}\frac{dN^{J/\psi}}{dM} + n_{\psi'}\frac{dN^{\psi'}}{dM}$$

where $n_{D\overline{D}}$, n_{DY}, $n_{J/\psi}$ and $n_{\psi'}$ are the normalisation factors whose value is determined in the fit and $dN^{D\overline{D}}/dM$, dN^{DY}/dM, $dN^{J/\psi}/dM$, $dN^{\psi'}/dM$ are the Monte-Carlo fitting functions obtained as outlined in chapter 4. dN^{bck}/dM is the function resulting from the fit of the combinatorial background mass distribution and R_{BCK} is the background normalisation factor calculated as detailed in chapter 5. Finally, dN^{+-}/dM is the experimental opposite-sign mass distribution which has to be fitted.

In chapter 4 the Monte-Carlo mass distributions have been fitted with ad-hoc functions whose parameter values are typical of the system and set-up for which the Monte-Carlo distributions have been generated. For each of the Monte-Carlo functionals, only the normalisation factor has been left unspecified, since it is then left as a free parameter in the fit of the experimental mass spectrum. In order to improve the quality of the fit, some other Monte-Carlo parameters can be freed in the fit of the experimental mass spectrum. In the present analysis, the following parameters are left *free*

- J/ψ, ψ', DY and $D\overline{D}$ normalisation factors.
- J/ψ mass and width, because the Monte-Carlo generated shape does not exactly reproduce the mass and width of the measured J/ψ.

and the following are *fixed*

- The ψ' mass and width, using the Monte-Carlo results for the J/ψ and ψ' mass difference and width ratio, i.e.,

$$M_{\psi'}^{data} = M_{J/\psi}^{data} + M_{\psi'}^{MC} - M_{J/\psi}^{MC} \tag{6.1}$$

  and

$$\sigma_{\psi'}^{data} = \sigma_{J/\psi}^{data}\frac{\sigma_{\psi'}^{MC}}{\sigma_{J/\psi}^{MC}} \tag{6.2}$$

- The R_{BCK} values calculated in chapter 5.

The signal mass distribution can be obtained subtracting the background contribution from the opposite-sign mass spectrum,

$$\frac{dN^{+-}_{signal}}{dM} = \frac{dN^{+-}}{dM} - R_{BCK}\frac{dN^{bck}}{dM} \tag{6.3}$$

The signal mass spectrum is then compared with the background subtracted opposite-sign fitting function, i.e.

$$\frac{dN^{+-}_{signal}}{dM} = n_{D\overline{D}}\frac{dN^{D\overline{D}}}{dM} + n_{DY}\frac{dN^{DY}}{dM} + n_{J/\psi}\frac{dN^{J/\psi}}{dM} + n_{\psi'}\frac{dN^{\psi'}}{dM} \tag{6.4}$$

6.3 $D\overline{D}/DY$ ratios from the fit of the mass spectra

The DY and $D\overline{D}$ normalisation factors found in the fit of the opposite-sign mass spectrum can be used to normalise the Monte-Carlo DY and $D\overline{D}$ functions in order to derive the ratio $D\overline{D}/DY$. Since the acceptance of the apparatus for DY pairs and for dimuons from the semi-leptonic decays of charmed pairs are different, the $D\overline{D}/DY$ ratio has to be acceptance corrected, i.e.

$$\frac{D\overline{D}}{DY} = \frac{\left\{\frac{n_{D\overline{D}}\int_{M_0}^{M_1}\frac{dN^{D\overline{D}}}{dM}dM}{A_{D\overline{D}}}\right\}}{\left\{\frac{n_{DY}\int_{M_0}^{M_1}\frac{dN^{DY}}{dM}dM}{A_{DY}}\right\}} \tag{6.5}$$

where $M_1 \leq 8\ GeV/c^2$ and M_0=1.5 GeV/c^2 or M_0=1.3 GeV/c^2. Even if starting the fit at M_0=1.5 GeV/c^2 excludes all possible contamination from the low mass resonances, when the lower starting point is used only a $\leq 2\%$ discrepancy is found on the $D\overline{D}/DY$ ratio. The values of the acceptances $A_{D\overline{D}}$ and A_{DY} have been listed in the last section of chapter 4. The Monte-Carlo $D\overline{D}$ fitting functions generated with m_c=1.5 GeV/c^2 are always used, unless differently specified.

Since the aim of the present work is the comparison of the $D\overline{D}/DY$ ratios obtained from the fit of the mass spectra with the expected $D\overline{D}/DY$, and since in the present chapter we only compare $D\overline{D}/DY$ ratios within the same nuclear system, the isospin correction (see chapter 1) can be neglected when dealing with the SU and PbPb systems. The energy and rapidity corrections, which are also needed when comparing cross sections measured for system covering a different rapidity region and for different energies, can also be neglected because of the above reason. On the other hand, when analysing the pA systems the isospin correction has to be taken into account because a common $D\overline{D}/DY$ is imposed in the fit, as explained in sec.6.8.

6.4 Fit of the PbPb mass spectra.

In fig.6.1 the fit of the 9 PbPb opposite-sign mass spectra, in the mass region 1.5 $< M < 7.0$ GeV/c^2, is shown. In fig.6.2 the fitting curves are superimposed on the signal mass spectra, after background subtraction. In fig.6.3 the same curves are superimposed on the IMR signal mass spectra. The extracted $D\overline{D}/DY$ ratios are listed in tab.6.1 together with the corresponding χ^2 of the fit; the associated $\simeq 10\%$ error is purely statistical.

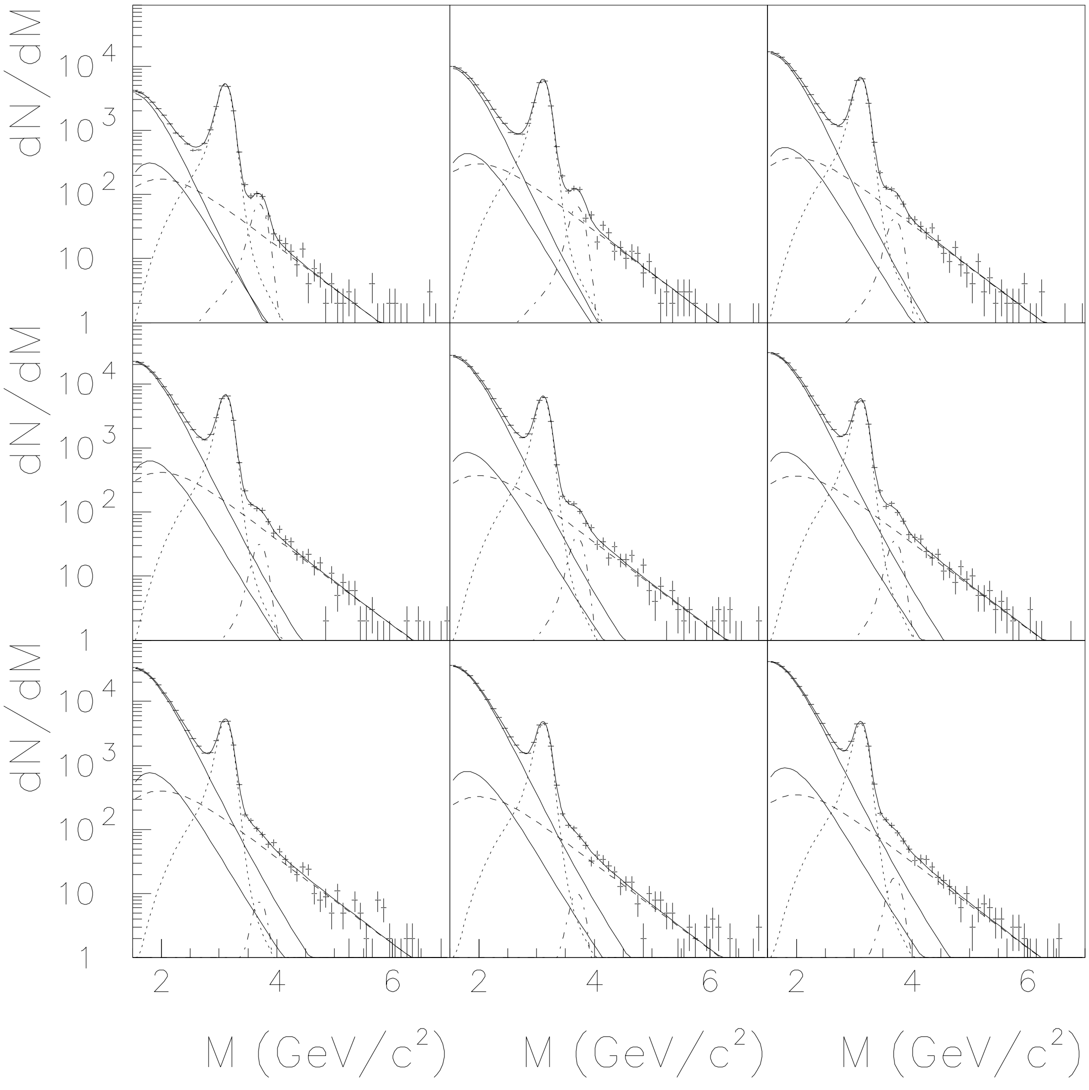

Figure 6.1: *Fit of the 9 PbPb opposite-sign mass distributions in the mass range 1.5< M <7.0 GeV/c^2.*

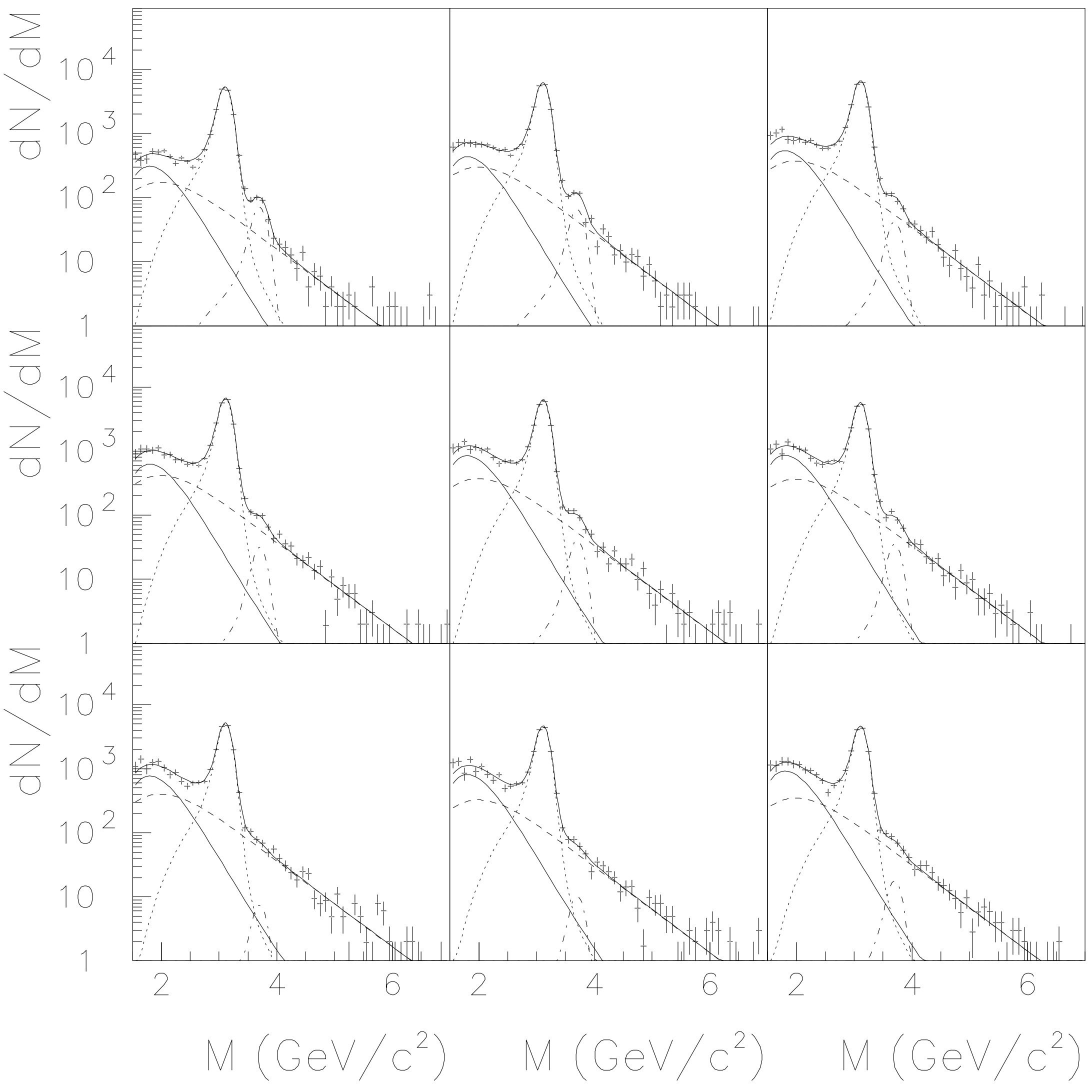

Figure 6.2: *PbPb signal mass distributions compared with the opposite-sign distribution fitting curves, after background subtraction.*

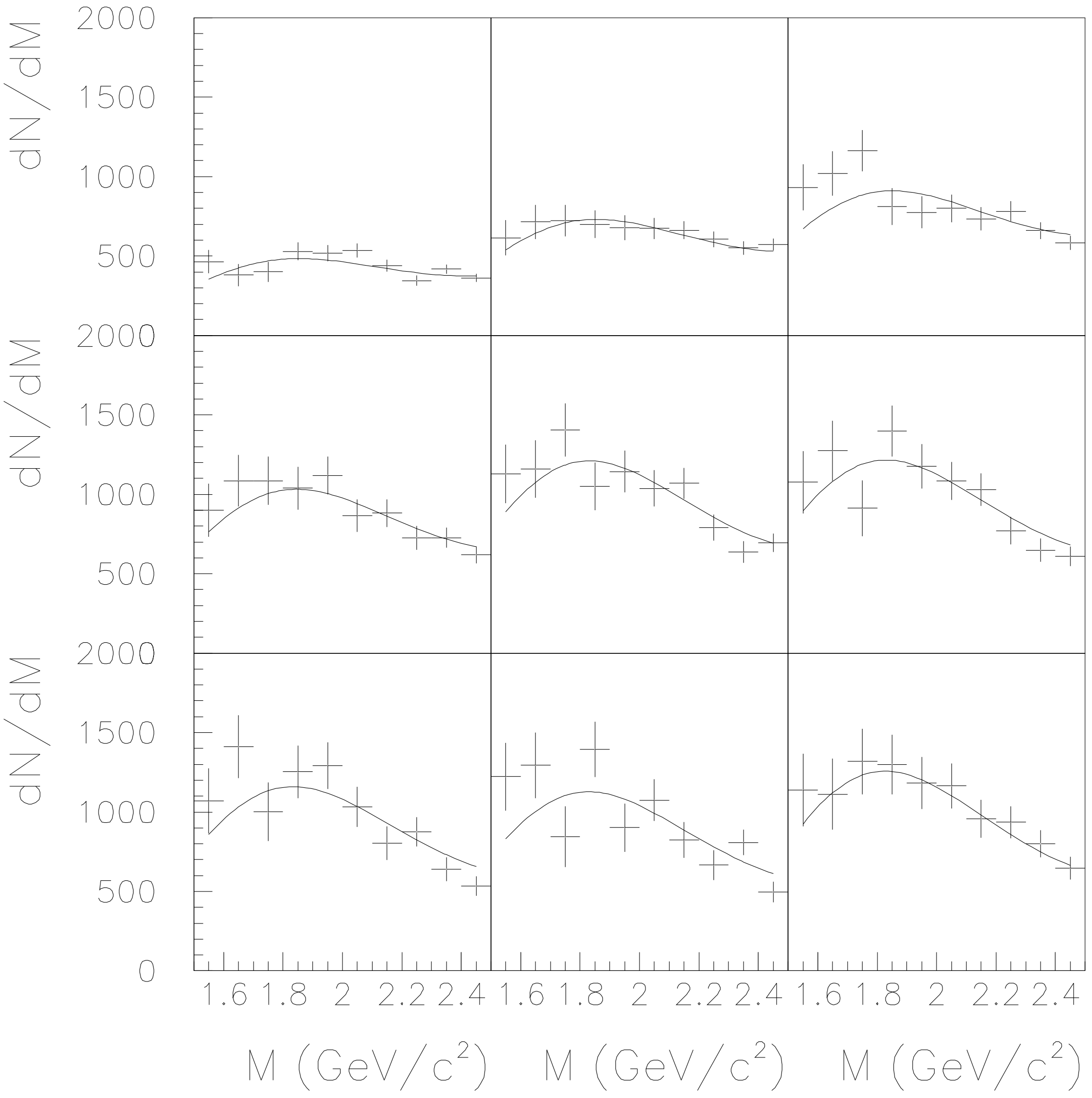

Figure 6.3: *PbPb signal mass distributions compared with the opposite-sign distribution fitting curves, after background subtraction. The IMR is shown.*

E_T bin	$\frac{D\overline{D}}{DY}$	χ^2
1	2.46 ± 0.32	1.9
2	2.01 ± 0.23	1.7
3	2.01 ± 0.22	1.6
4	2.10 ± 0.22	1.7
5	3.15 ± 0.29	1.5
6	3.27 ± 0.31	0.9
7	2.66 ± 0.27	1.7
8	3.46 ± 0.36	1.8
9	3.68 ± 0.37	0.8

Table 6.1: $D\overline{D}/DY$ *obtained when fitting the 9 PbPb mass spectra with* $R_{BCK} = R_{BCK}^{MC}$.

6.4.1 The charm mass

In chapter 4 the open charm differential distributions have been obtained with the PYTHIA event generator and for a charm mass value m_c=1.5 GeV/c^2. Since the adopted value of the charm mass influences the shapes of the generated distributions, the open charm differential distributions for the PbPb set-ups have been also generated with two alternative mass values in order to estimate the size of the induced effect.

From the comparison of the experimentally measured $c\overline{c}$ cross sections with leading order QCD calculations the charm mass value m_c=1.5 GeV/c^2 seems to be favoured (see chapter 1 and reference therein). When the value m_c=1.2 GeV/c^2 is used, a reasonable agreement between the measured cross sections and the QCD calculations still exists but the theoretical predictions clearly tend to overestimate the experimentally measured cross sections. On the other hand, when using m_c=1.8 GeV/c^2 the QCD calculations clearly underestimate the measured cross sections. Thereafter, I here assume that the actual charm mass value can range from 1.2 up to 1.5 GeV/c^2 and investigate the effect of the related incertitude on the $D\overline{D}/DY$ ratios. Tab.6.2 lists the $D\overline{D}/DY$ ratios obtained when the PbPb mass spectra are fitted with the Monte-Carlo $D\overline{D}$ fitting functions corresponding to the three different charm mass values. The discrepancy between the ratios obtained when using the two extreme charm mass values is $\simeq$15% , whilst it is $\leq$4% when the values m_c=1.5 and 1.35 GeV/c^2 are used. In the present analysis the value m_c=1.5 GeV/c^2 has been adopted. The above systematic incertitude on the $D\overline{D}/DY$ ratios affects all the ratios in the same direction and is therefore never explicitly included.

E_T bin	$\frac{D\overline{D}}{DY}$	$\frac{D\overline{D}}{DY}$	$\frac{D\overline{D}}{DY}$
	$m_c = 1.5GeV/c^2$	$m_c = 1.35GeV/c^2$	$m_c = 1.2GeV/c^2$
1	2.46 ± 0.32	2.55 ± 0.32	2.83 ± 0.36
2	2.01 ± 0.23	2.09 ± 0.24	2.33 ± 0.27
3	2.01 ± 0.22	2.07 ± 0.23	2.36 ± 0.26
4	2.10 ± 0.22	2.15 ± 0.23	2.45 ± 0.26
5	3.15 ± 0.29	3.24 ± 0.30	3.66 ± 0.34
6	3.27 ± 0.31	3.35 ± 0.32	3.80 ± 0.36
7	2.66 ± 0.27	2.72 ± 0.27	3.10 ± 0.31
8	3.46 ± 0.36	3.54 ± 0.36	4.04 ± 0.42
9	3.68 ± 0.37	3.75 ± 0.37	4.27 ± 0.43

Table 6.2: $D\overline{D}/DY$ *obtained when the 9 PbPb opposite-sign mass distributions are fitted with the three different* $D\overline{D}$ *Monte-Carlo functionals corresponding to the 3 quoted values of* m_c.

6.5 Fit of the SU mass spectra

The analysis of the SU data has been performed in the same way as for the PbPb system. In fig.6.4 the fits of the 5 SU opposite-sign mass spectra are shown. In fig.6.5 the background subtracted fitting curves have been superimposed on the signal mass spectra. The same is shown in fig.6.6 for the IMR only. In tab.6.3 the extracted $D\overline{D}/DY$ ratios are listed together with the corresponding χ^2 of the fit. The associated $\simeq 10\%$ error is purely statistical.

E_T bin	$\frac{D\overline{D}}{DY}$	χ^2
1	1.62 ± 0.15	2.2
2	1.66 ± 0.14	1.6
3	1.95 ± 0.15	2.0
4	2.42 ± 0.13	1.4
5	2.07 ± 0.17	1.1

Table 6.3: $D\overline{D}/DY$ *obtained when fitting the SU opposite-sign mass spectra with the Monte-Carlo* R_{BCK} *values.*

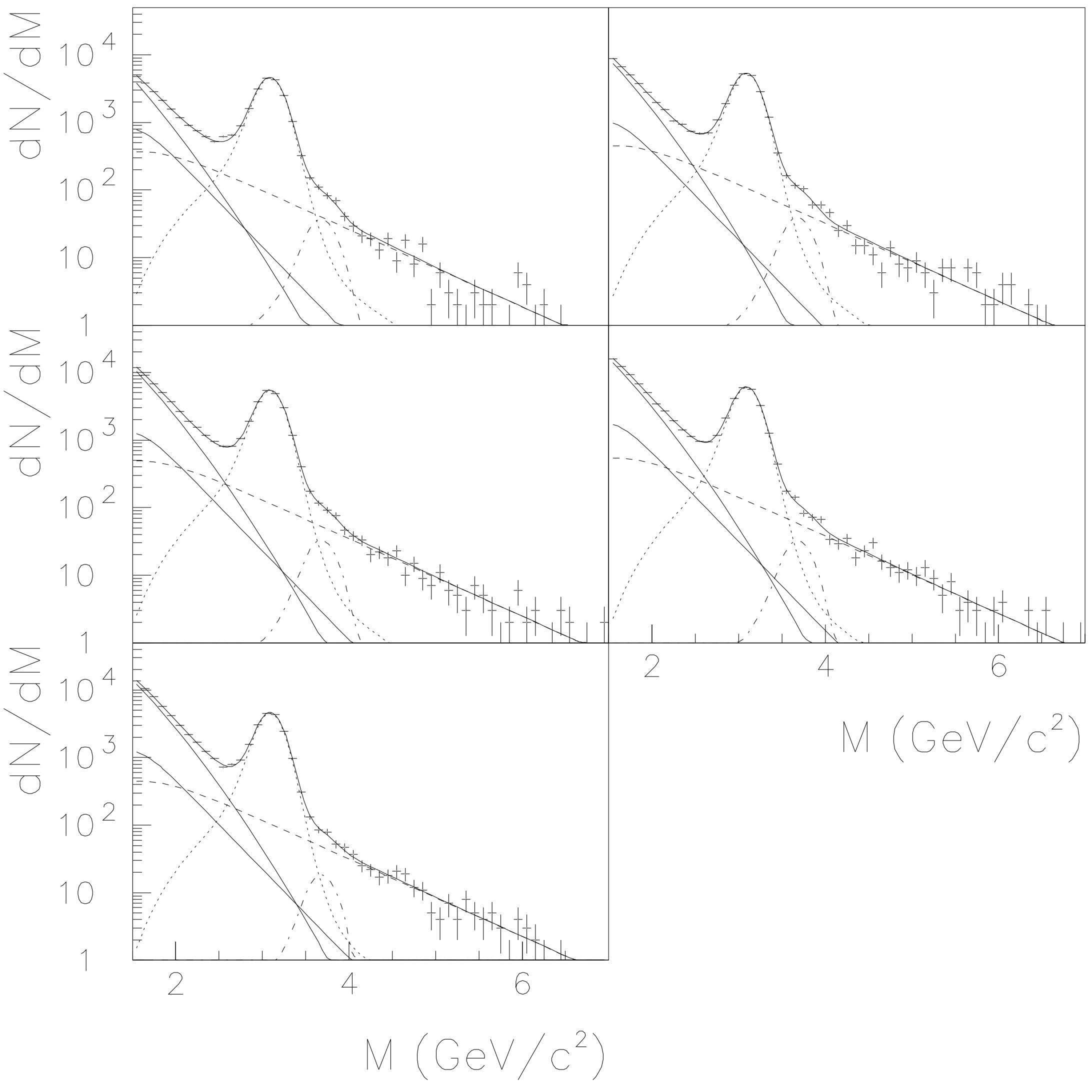

Figure 6.4: *Fit of the 5 SU opposite-sign mass distributions in the mass range 1.5< M <7 GeV/c^2.*

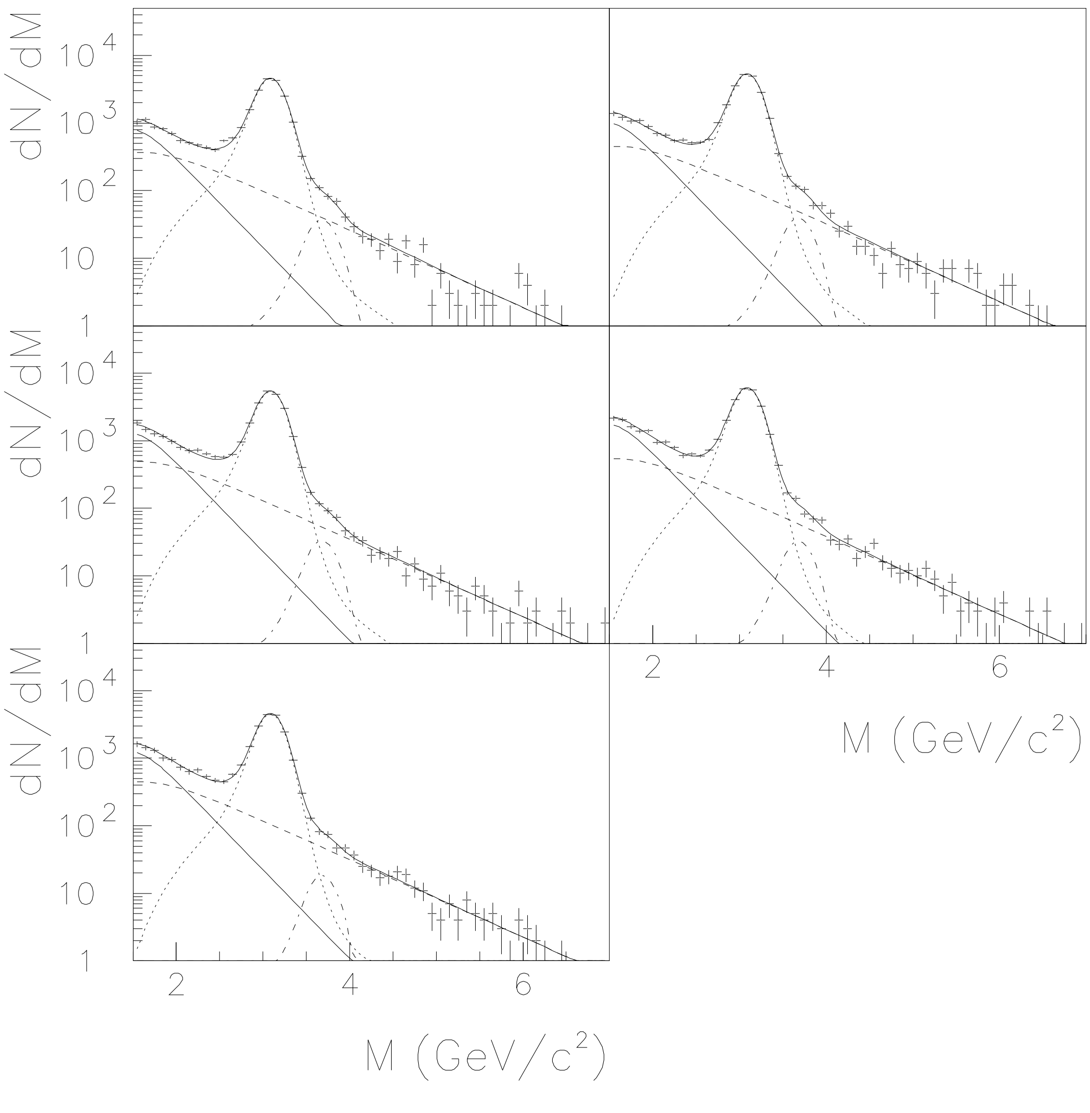

Figure 6.5: *SU signal mass distributions compared with the opposite-sign mass spectra fitting curves, after background subtraction.*

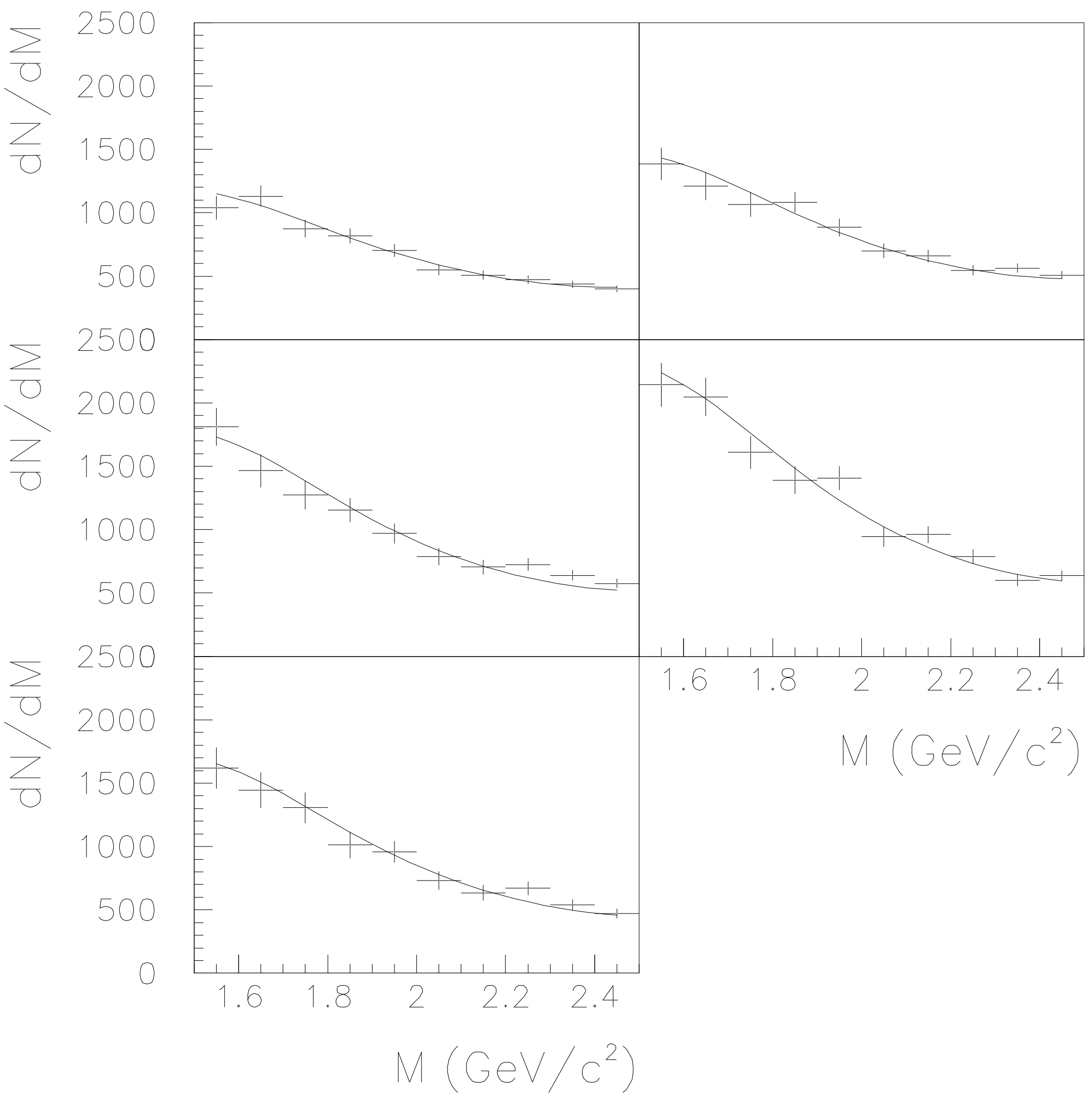

Figure 6.6: *SU signal mass distributions compared with the opposite-sign mass spectra fitting curves, after background subtraction. The IMR is shown.*

6.6 PbPb and SU results

When the $D\overline{D}$ contribution is left as a free parameter in the fit of the opposite-sign mass spectra and the background normalisation is fixed by the Monte-Carlo R_{BCK} values, a satisfactory description of all the mass spectra is achieved. The $D\overline{D}/DY$ is enhanced by a factor $\simeq 1.3$ in central S-U and $\simeq 1.8$ in central Pb-Pb interactions with respect to peripheral collisions. In fig.6.7 the $D\overline{D}/DY$ obtained from the fit of the SU and PbPb mass spectra are plotted as a function of the transverse energy E_T.

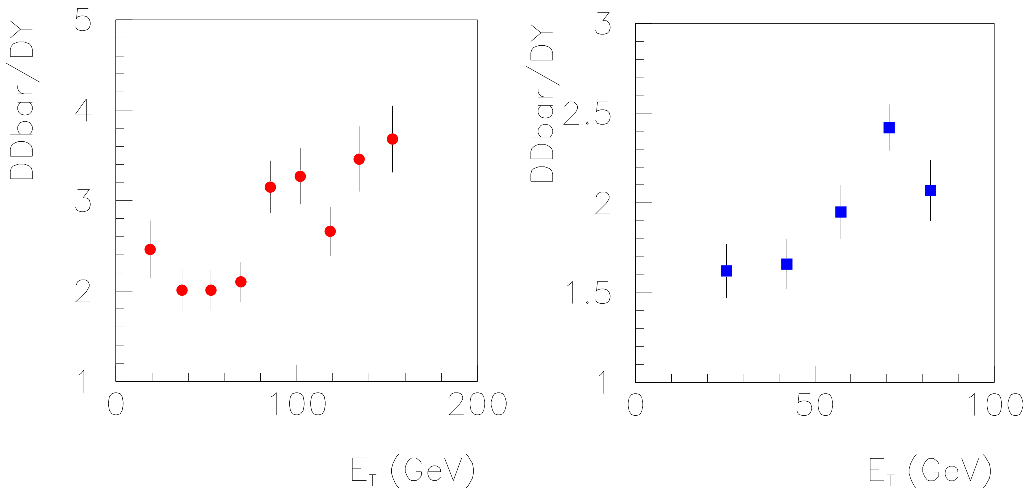

Figure 6.7: *The $D\overline{D}/DY$ ratios obtained when fitting the PbPb (left) and SU (right) mass spectra is plotted vs. the transverse energy E_T. No isospin correction has been applied.*

6.7 The p_T, cosθ, y differential distributions

To support the hypothesis that the IMR excess found in A-B collisions originates from an enhanced $D\overline{D}$ production, the p_T, cosθ and y differential distributions in the IMR can be studied. The p_T, cosθ and y differential distributions for the DY, $D\overline{D}$ and J/ψ are generated as described in chapter 4. The Monte-Carlo shapes are then (separately) normalised using the results of the fits of the mass spectra,

$$\int_0^{V_{max}} \frac{dN^{MC}}{dV} dV = \int_{1.5}^{2.5} \frac{dN}{dM} dM \text{ (with V=}p_T\text{, cos}\theta\text{, } y) \tag{6.6}$$

where V_{max} is the maximum value of the considered variable in the corresponding Monte-Carlo distribution for 1.5< M <2.5 GeV/c^2.
The enhanced $D\overline{D}$ contribution is therefore already included in the adopted normalisation. The resulting curves are then *superimposed* on the experimental distributions for 1.5< M <2.5 GeV/c^2.
The DY and $D\overline{D}$ Monte-Carlo p_T distributions clearly have different shapes, as visible in fig.6.8 where the experimental p_T distributions are shown for four of the PbPb bins, together with the superimposed Monte-Carlo curves after normalisation. On the other hand, in the cosθ and y distributions the shapes of the two contributions can not be easily distinguished, as shown in fig.6.11. The p_T distribution can be therefore used in order to support the results of the analysis of the mass spectra.

In fig.6.8 the most peripheral bins are better described by the Monte-Carlo shapes than the more central ones. The Monte-Carlo shapes used in fig.6.8 have been generated as detailed in chapter 4, where the value σ_{k_T}=0.8 GeV/c has been imposed. In chapter 4, the open charm differential distributions have been generated with PYTHIA, where the transverse momentum of the muon pair originates from the intrinsic transverse momentum k_T associated to the colliding partons. On the other hand, the DY and high mass resonances p_T differential distributions have been generated with the following parametrisation,

$$\frac{d\sigma}{dp_T} \propto p_T m_T K_1(\frac{m_T}{T}) \tag{6.7}$$

where K_1 is the first order modified Bessel function, i.e

$$K_1(\frac{m_T}{T}) = \frac{e^{-(m_T/T)}}{\sqrt{(m_T/T)}} \cdot P_6(T/m_T) \tag{6.8}$$

In order to check whether a better description of the p_T differential distributions can be obtained when also the DY and high mass resonances are generated with PYTHIA, the Monte-Carlo generation has been repeated using the PYTHIA 5.7 event generator with the MRS 43 parton distribution function[3] for *all* the contributing processes.

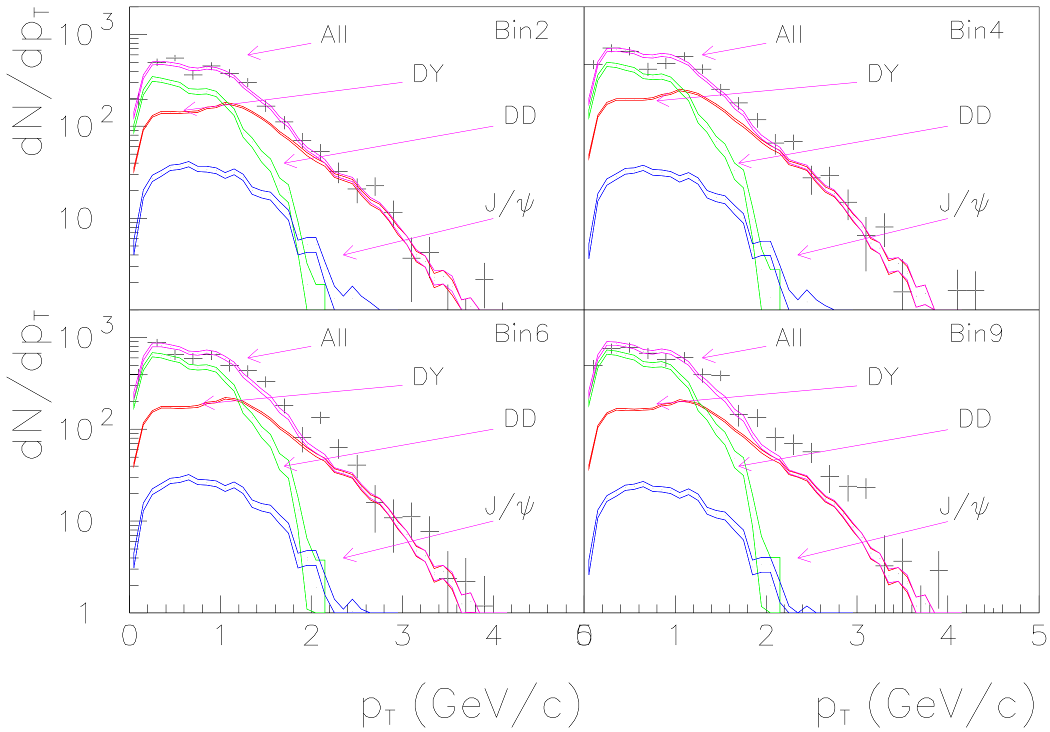

Figure 6.8: *PbPb p_T differential distribution for $1.5 < M < 2.5$ GeV/c^2 compared with the normalised Monte-Carlo predictions. The Monte-Carlo generation has been done as described in chapter 4, with σ_{k_T}=0.8 GeV/c. From top-left to bottom-right, 4 E_T bins with increasing centrality are shown.*

6.7.1 PYTHIA p_T distributions.

In chapter 4, the open charm has been generated with PYTHIA using the Gaussian intrinsic transverse momentum distribution with σ_{k_T}=0.8 GeV/c. The latter had in fact already been used in the SU analysis performed in ref.[1] whose Monte-Carlo shapes we directly use; we therefore adopted the same parametrisations for the pA and PbPb systems.

In the following, the 4 different (and reasonable) values σ_{k_T}=0.6, 0.8, 0.9, 1.0 GeV/c, are used to generate the DY, $D\overline{D}$ and J/ψ Monte-Carlo differential distributions. As shown in fig.6.9 for the PbPb system, the $D\overline{D}$ mass shape distribution is not particularly affected by changing the σ_{k_T} value, whilst the IMR DY shape is particularly sensitive to it. In fig.6.10 the DY Monte-Carlo shape as obtained in chapter 4 is compared with the PYTHIA generated ones and it turns out to be quite similar to the one generated with σ_{k_T}=0.8 GeV/c; the integrals of the two functions in the mass region 1.5< M <2.5 GeV/c^2 differ by $\simeq$ 7%.
The best value of σ_{K_T} is the one which leads to a better reproduction of all the mass, p_T, cosθ and y differential distributions. The mass differential distribution can not discriminate because in the high mass region, where for M > 4.5 GeV/c^2 only DY dimuons can be found, the DY Monte-Carlo shape does not sensibly change with changing k_T. The $cos\theta$ and rapidity distributions are also ruled out, since the dimuon contributions from DY, $D\overline{D}$ and J/ψ change with the chosen σ_{k_T} but the superposition of the 3 processes always gives a good description of the data, as shown in fig.6.11 for the most central PbPb E_T bin.
In fig.6.12, the Monte-Carlo generated p_T distributions are shown to be strongly affected by a change in the σ_{k_T} value. It is therefore on the basis of the results of the analysis of the p_T spectra that the best σ_{K_T} has to be chosen.

In fig.6.13 the PbPb DY and $D\overline{D}$ shapes corresponding to different σ_{k_T} values are compared.
From fig.6.12 it is clear that the best data reproduction is obtained when imposing σ_{k_T} = 0.9 GeV/c. This has been checked for all the 9 PbPb E_t bins. In fig.6.14, 6.15, 6.16 the experimental p_T, $cos\theta$ and y differential distributions for 4 representative PbPb E_t bins are compared with the normalised Monte-Carlo shapes for σ_{k_T} = 0.9 GeV/c.

6.7.2 Results

A good description of the p_T, y and $cos\theta$ distributions for the SU and PbPb systems has been obtained in the hypothesis that the excess measured in the previous section originates from an enhanced open charm production. Therefore, since no additional hypothesis have been introduced, the study of the p_T (y and $cos\theta$) spectra supports the given interpretation of the measured IMR excess.

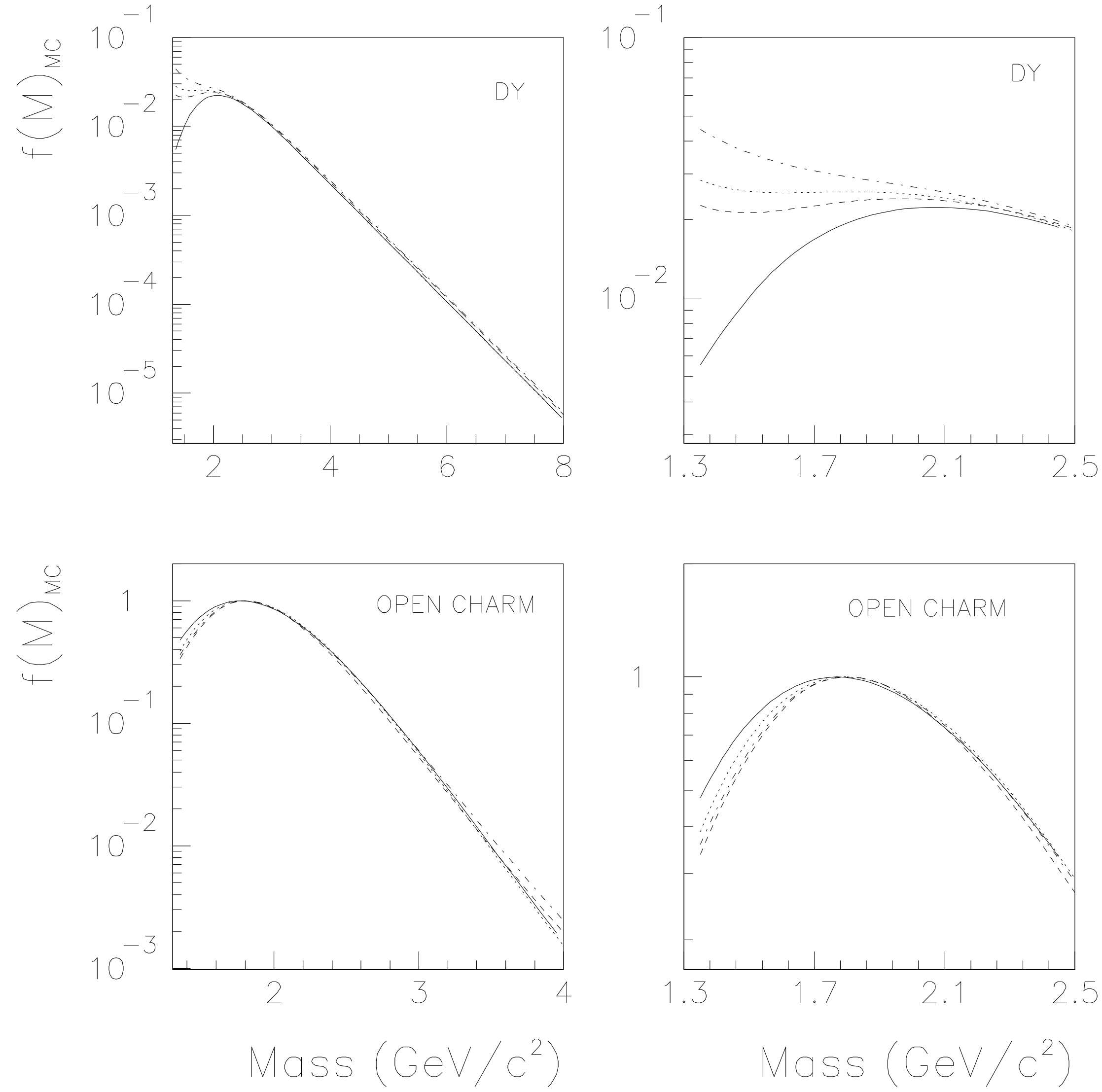

Figure 6.9: *Comparison of fitting function shapes for DY (top) and open-charm (bottom) obtained when fitting the Monte-Carlo shapes generated with PYTHIA and* σ_{k_T}*=0.6 GeV/c (full line), 0.8 GeV/c (dashed line), 0.9 GeV/c (dotted line), 1.0 GeV/c (dash-dotted line). The whole mass region (left) and the IMR (right) are shown.*

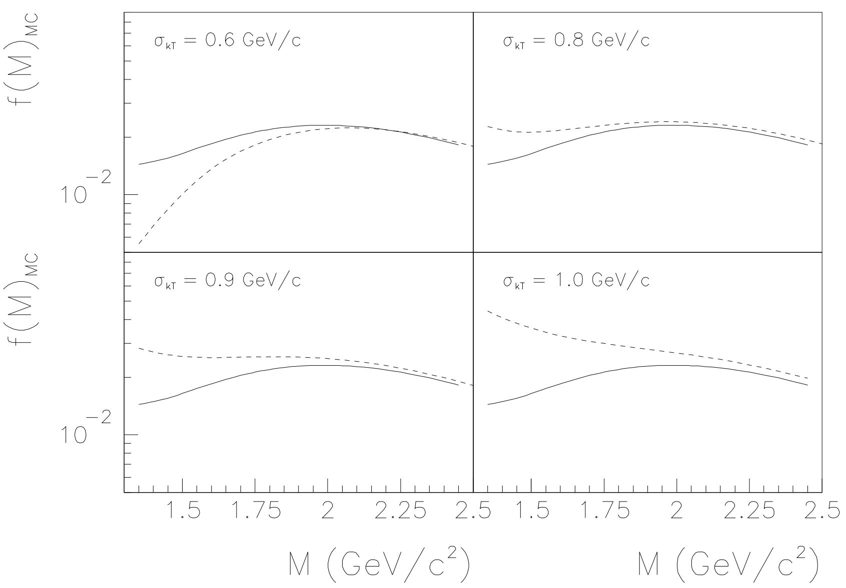

Figure 6.10: *Comparison of the PbPb Monte-Carlo DY fitting function shape obtained in chapter 4 (full line) with the ones obtained with PYTHIA and* σ_{k_T}*=0.6,0.8,0.9,1.0 GeV/c (dashed line).*

6.7.3 Fit of the mass spectra (revisited)

In the previous subsection we have seen that a nice agreement can be reached between the experimental and Monte-Carlo p_T, y and $cos\theta$ distributions if the PYTHIA event generator is used to generate all the processes contributing to the IMR, with σ_{K_T}=0.9 GeV/c. In order to establish the normalisation factors for the Monte-Carlo p_T, cosθ and y distributions, the mass distributions have been fitted with the Monte-Carlo mass shapes generated with the same σ_{K_T}. The corresponding $D\overline{D}/DY$ ratios have been therefore obtained. In tab.6.4, the $D\overline{D}/DY$ values obtained for the 9 PbPb E_T bins when using the PYHTIA generator with σ_{k_T} = 0.9 GeV/c, are compared with the previous ones. The difference between the two sets of values is smaller than the error on the $D\overline{D}/DY$ values ($\leq$ 13%). Since the SU $D\overline{D}/DY$ are affected by a similar error ($\leq$ 10%) and since the Monte-Carlo generation of all the needed processes with PYTHIA is extremely CPU time consuming, the $D\overline{D}/DY$ ratios extracted when using the set of Monte-Carlo shapes obtained in chapter 4 will be used in the following, both for the PbPb and the SU data sets. On the other hand, the pA sets of data discussed in the next section are characterised by a larger statistics in the IMR and are therefore more sensitive to small changes in the Monte-Carlo fitting function shapes. This has been verified analysing the pA data with both the Monte-Carlo fitting functions obtained with σ_{k_T}=0.9 GeV/c and with the ones obtained when using σ_{k_T}=0.8 GeV/c. When the latter is used the quality of the fit is poor and the $D\overline{D}/DY$ value strongly depends on the fitting procedure.

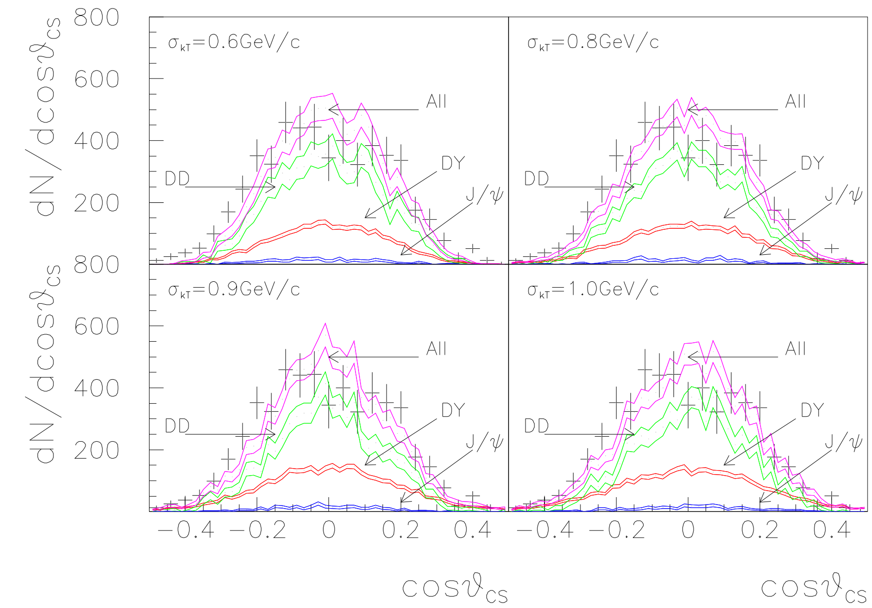

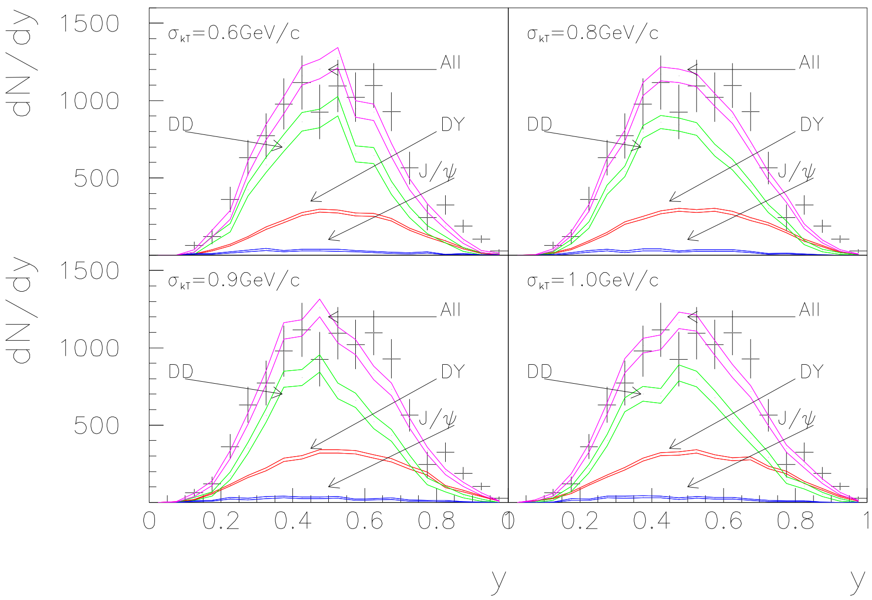

Figure 6.11: *PYTHIA generated* $cos\theta$ *and* y *differential distributions in the IMR (1.5* $< M <$ *2.5 GeV/*c^2*) for the indicated 4* σ_{k_T} *values, compared with the experimental PbPb* $cos\theta$ *and* y *distributions in the same mass region and for the most central* E_T *bin.*

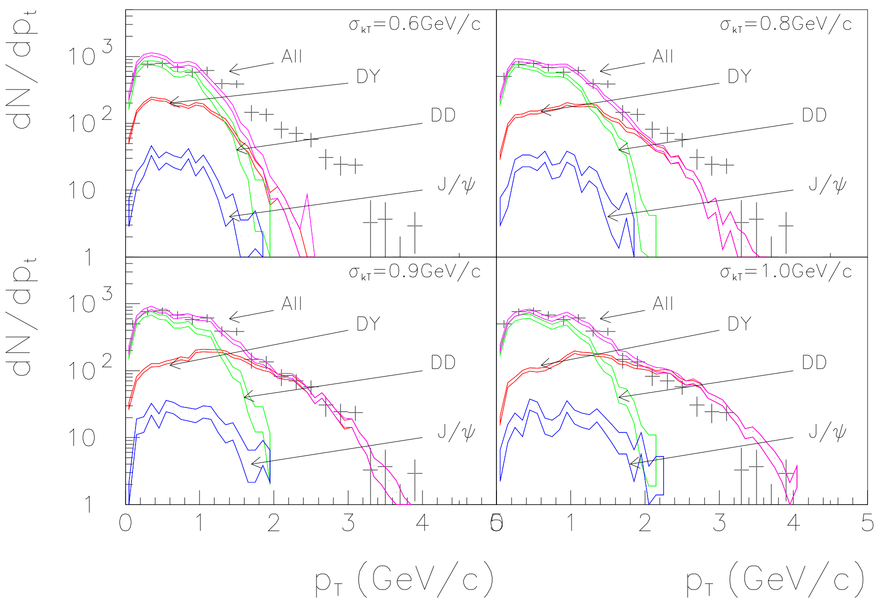

Figure 6.12: *IMR (1.5 < M < 2.5 GeV/c^2) p_T differential distribution for the PbPb most central bin, compared with the PYTHIA generated p_T distributions for the 4 indicated σ_{k_T} values.*

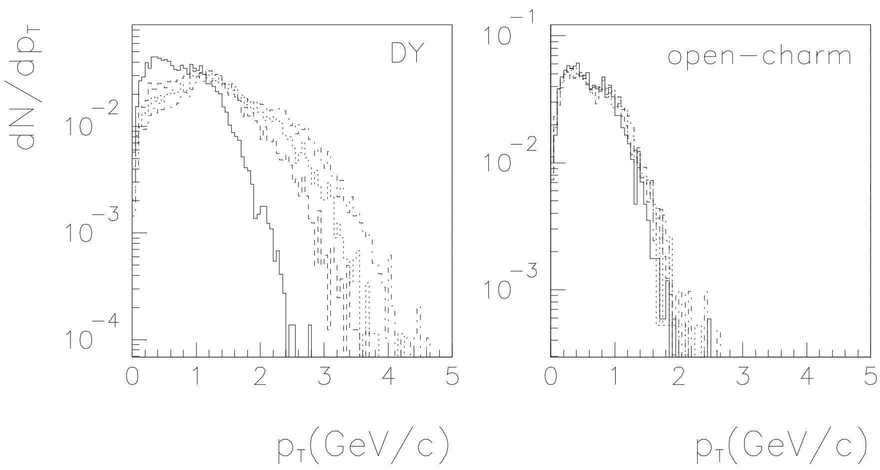

Figure 6.13: *PYTHIA generated DY (left) and $D\overline{D}$ (right) p_T differential distributions for σ_{k_T}=0.6,0.8,0.9,1.0 GeV/c. The larger the σ_{k_T} value, the more the DY distribution spreads towards higher p_T. The $D\overline{D}$ distribution does not show any strong k_T dependence.*

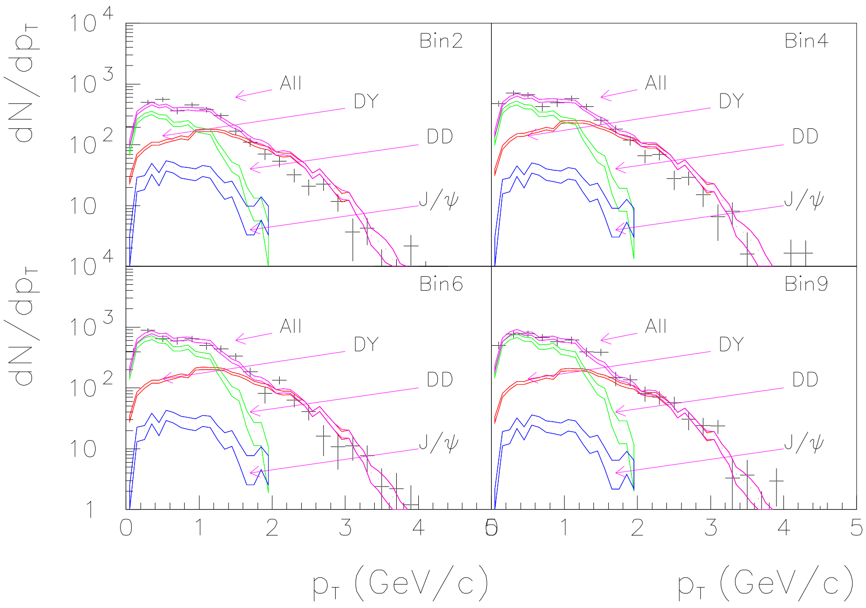

Figure 6.14: *PbPb p_T differential distributions for* $1.5 < M < 2.5$ *GeV/c^2 compared with the PYTHIA predictions for σ_{k_T} = 0.9 GeV/c. From top-left to bottom-right, 4 E_T bins corresponding to increasing centrality are shown.*

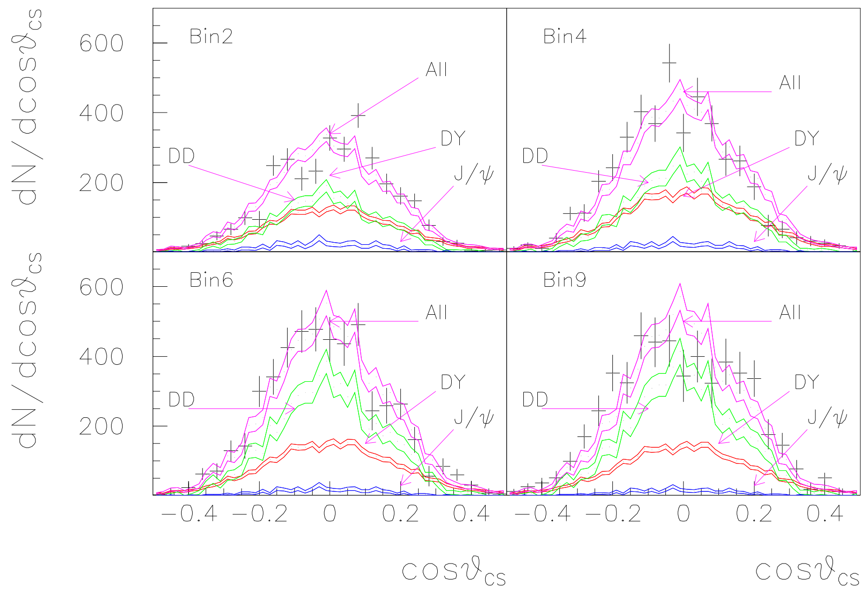

Figure 6.15: *PbPb cosθ differential distributions for* $1.5 < M < 2.5$ *GeV/c^2 compared with the PYTHIA predictions for σ_{k_T} = 0.9 GeV/c. From top-left to bottom-right, 4 E_T bins corresponding to increasing centrality are shown.*

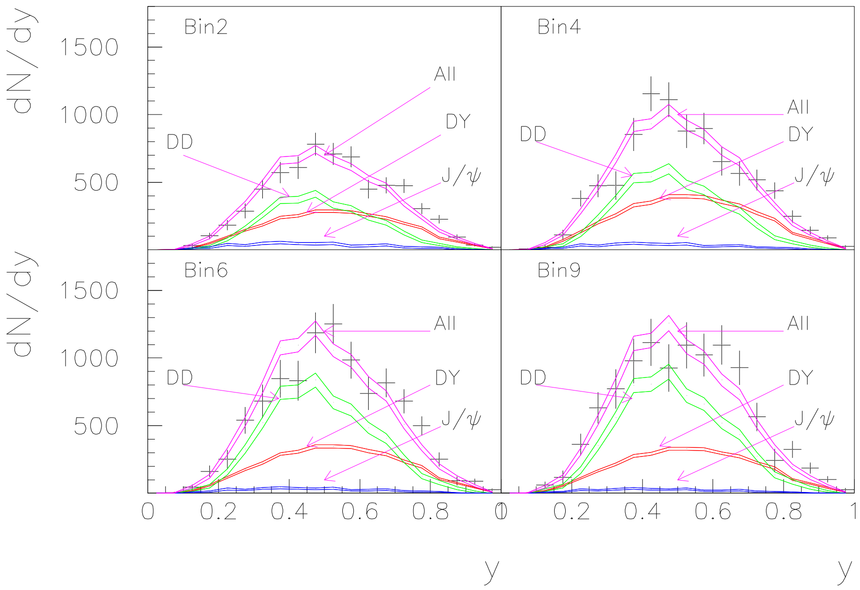

Figure 6.16: *PbPb rapidity differential distributions for* $1.5 < M < 2.5$ *GeV/c^2 compared with the PYTHIA predictions for* σ_{k_T} *= 0.9 GeV/c. From top-left to bottom-right, 4* E_T *bins corresponding to increasing centrality are shown.*

Thereafter, the pA analysis presented in the following has been performed using the Monte-Carlo fitting functions obtained with σ_{k_T}=0.9 GeV/c.

	PREVIOUS ANALYSIS		PYTHIA $\sigma_{k_T} = 0.9$ GeV/c	
E_T bin	$\frac{D\overline{D}}{DY}$	χ^2	$\frac{D\overline{D}}{DY}$	χ^2
1	2.46 ± 0.32	1.9	2.67 ± 0.30	2.9
2	2.01 ± 0.23	1.7	2.15 ± 0.25	2.9
3	2.01 ± 0.22	1.6	2.05 ± 0.25	1.8
4	2.10 ± 0.22	1.7	2.12 ± 0.24	1.8
5	3.15 ± 0.29	1.5	3.22 ± 0.31	1.5
6	3.27 ± 0.31	0.9	3.36 ± 0.30	1.0
7	2.66 ± 0.27	1.7	2.64 ± 0.28	1.8
8	3.46 ± 0.36	1.8	3.45 ± 0.38	1.8
9	3.68 ± 0.37	0.8	3.71 ± 0.39	1.0

Table 6.4: *$D\overline{D}/DY$ values and χ^2's obtained from the fit of the 9 PbPb mass spectra corresponding to the 9 PbPb E_T bins. The previous values are compared with the ones obtained using PYTHIA to generate all the Monte-Carlo shapes, with a Gaussian k_T distribution and σ_{k_T} = 0.9 GeV/c.*

6.8 Fit of the pA mass spectra

Since no IMR dimuon excess has been measured in pA collisions, the dimuon yield measured in pA interactions can be taken as a reference when studying nucleus-nucleus systems. The analysis of the pA data is therefore particularly important when the absolute value of the IMR excess observed in nucleus-nucleus collisions has to be determined.

Both the DY and the $D\overline{D}$ cross sections have been verified to linearly scale with A in pA interactions (see chapter 1). This implies that, when isospin corrections have been applied, a constant $D\overline{D}/DY$ ratio is expected in p-A collisions for any value of the target atomic number. Therefore, since the four pA sets of data have been collected with identical set-ups, except for the target material and length, a common isospin corrected $D\overline{D}/DY$ can be imposed and a simultaneous fit can be performed on the four mass spectra. Tab.6.5 lists the isospin correction factors I_{DY} (see chapter 1) calculated for the MRS A set of parton distribution functions and for M>1.5 GeV/c^2, -0.5< $cos\theta$ <0.5 and -0.52< y <0.48.
The simultaneous fit can be performed either on the whole mass spectra, including the high mass resonances contributions, or excluding the high mass resonances from the fit in order to reduce the number of free parameters. In the following both approaches are discussed and the results are subsequently compared.

System	Energy (GeV)	A	Z	I_{DY}
pAl	450	27	13	0.982
pCu	450	63	29	0.981
pAg	450	108	47	0.980
pW	450	184	74	0.978

Table 6.5: *Isospin correction factors for the DY, calculated for 450 GeV/c pA(A=Al, Cu, Ag, W) interactions with the MRS A set of PDF and for M>1.5 GeV/c^2, -0.5< $cos\theta$ <0.5 and -0.52< y <0.48.*

6.8.1 Fit of the whole mass spectra

When fitting the mass spectra in the mass range 1.5 (1.3) $< M <$ 8.0 GeV/c^2, 21 parameters are left free, i.e, the 4 DY, 4 J/ψ and 4 ψ' normalisation factors, the 4 J/ψ masses and the 4 J/ψ widths, and the common $D\overline{D}/DY$.

In fig.6.17 the result of the simultaneous fit of the 4 pA data is shown. In fig.6.18 the corresponding signal mass distributions are compared with the curves resulting from the fit of the opposite-sign mass spectra, after background subtraction. In fig.6.19 the signal distributions in the IMR can be better seen. We find

$$\frac{D\overline{D}}{DY} = 4.09 \pm 0.06 \ (\chi^2{=}3.4) \tag{6.9}$$

6.8.2 Fit of a restricted mass range

When fitting the restricted range of mass between 1.3 $< M <$ 2.0 and 4.5 $< M <$ 8.0 GeV/c^2, only 5 parameters are left free, i.e., the 4 DY normalisation factors and the common $D\overline{D}/DY$.

In fig.6.20 the result of the simultaneous fit of the 4 pA data sets in the restricted mass region is shown. In fig.6.21 the signal mass distributions are compared with the fitting curves, background subtracted. In fig.6.22 the corresponding IMR signal mass distributions are shown. We find

$$\frac{D\overline{D}}{DY} = 4.36 \pm 0.09 \ (\chi^2{=}1.6) \tag{6.10}$$

The quality of the fit has improved with respect with the previous approach, and the $D\overline{D}/DY$ values differ by $\simeq$6% only.

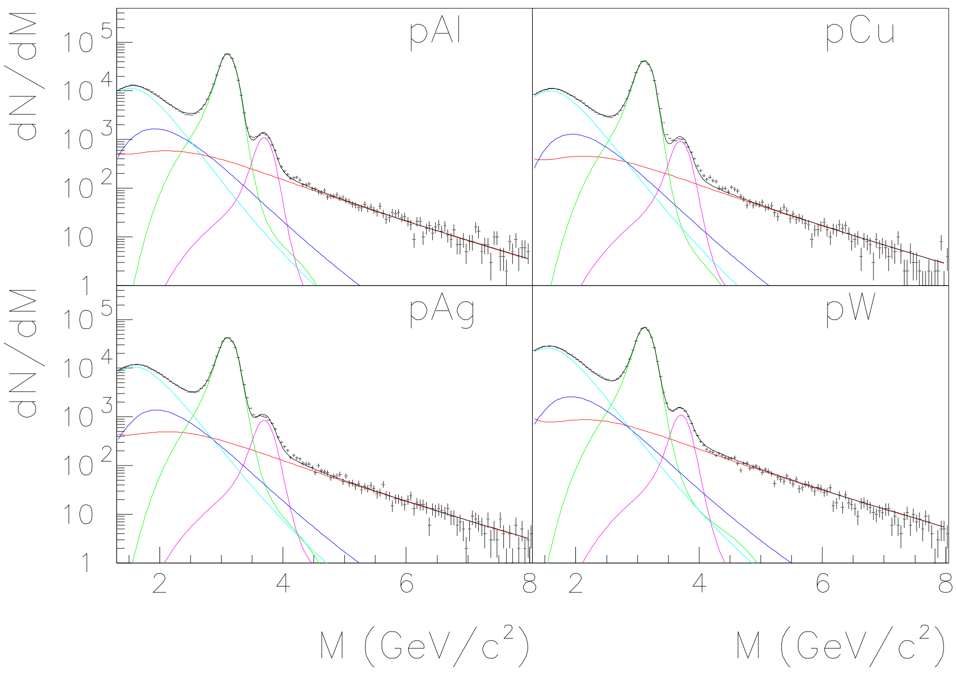

Figure 6.17: *Simultaneous fit of the 4 pA data sets in the whole mass range, 1.3< M <8.0 GeV/c^2. The nominal Monte-Carlo R_{BCK} values have been imposed.*

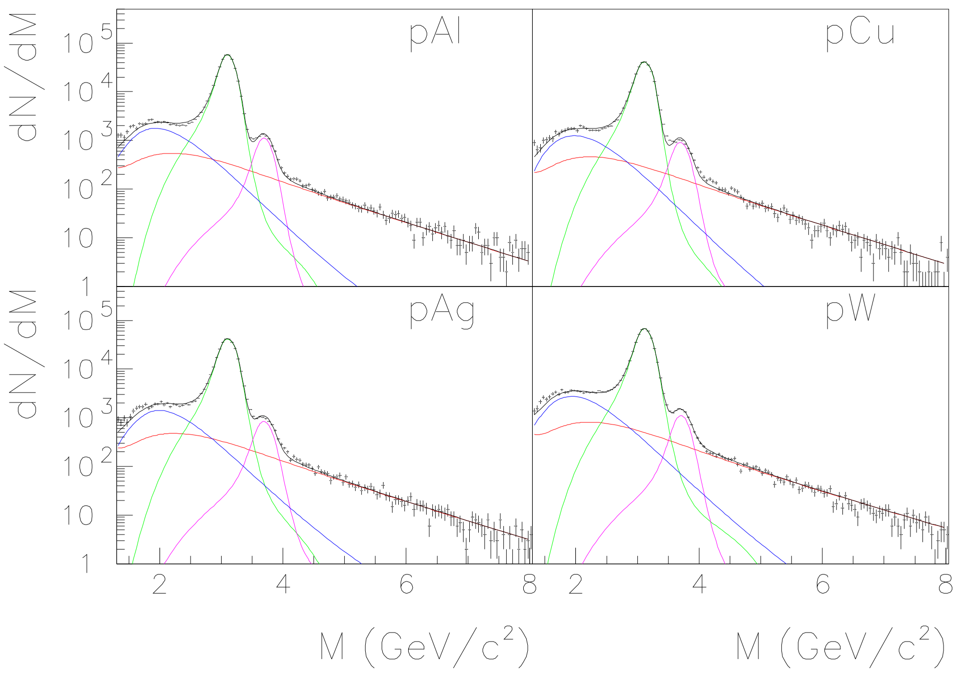

Figure 6.18: *Signal mass distributions compared with the curves resulting from the fit of the opposite-sign distributions shown in the previous figure, after background subtraction.*

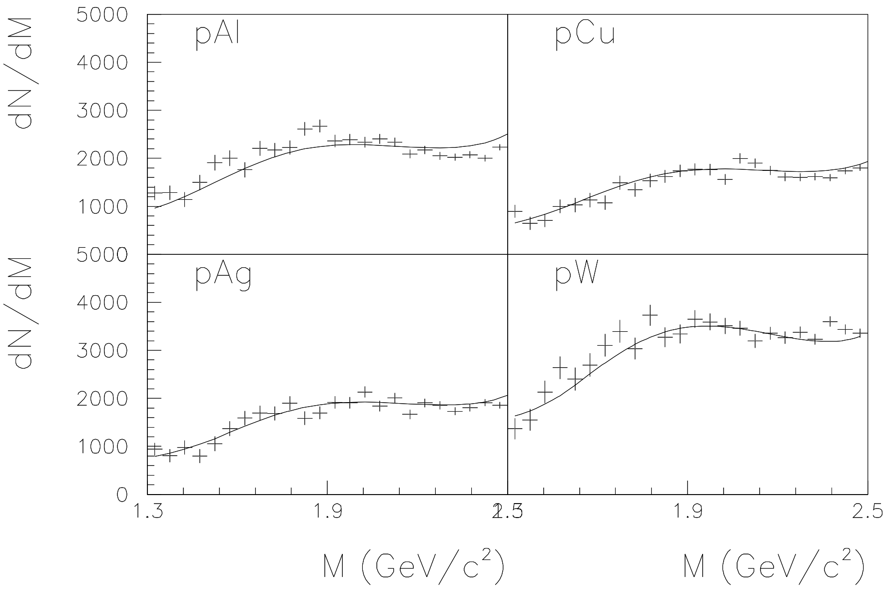

Figure 6.19: *Signal mass distributions compared with the curves resulting from the fit of the opposite-sign distributions shown in the previous figure, after background subtraction. The IMR is shown.*

6.8.3 pA : results and discussion

We have seen that the $D\overline{D}/DY$ ratios obtained for the 4 pA data with the two above different approaches differ by only $\simeq$6%. The larger χ^2 found in the first approach is probably due to the inclusion of the high mass resonances region, where, in order to have a small number of free parameters, the fit has not been optimised. For instance, if the widths of the 4 ψ' were freed, the quality of the fits at the ψ' level would improve (and so the overall χ^2), but the quality of the fit in the IMR would be the same. We then calculate the pA $D\overline{D}/DY$ reference value as the weighted average of the values given in eq.6.9 and eq.6.10. The incertitude associated with the average value is given by the maximum distance between the average value itself and the ones in eq.6.9 and eq.6.10, when the statistical error on the latter is taken into account. We therefore have

$$\frac{D\overline{D}}{DY}\Big|_{pA}^{450GeV/c} = 4.20 \pm 0.25 \tag{6.11}$$

6.8.4 The pA p_T, cosθ and y distributions

In sec.6.7 the p_T, $cos\theta$ and y differential distributions of the SU and PbPb systems in the IMR region have been studied and it has been found that they can be well reproduced if PYTHIA is used to generate the Monte-Carlo shapes for all the contributing processes with σ_{k_T}=0.9 GeV/c. In the previous part of the present section,

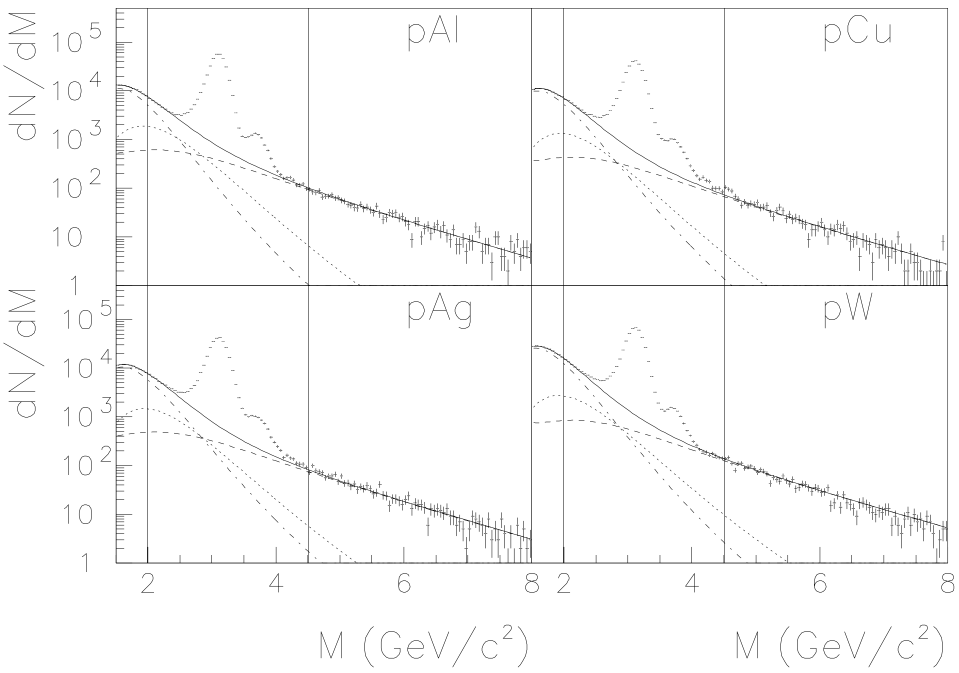

Figure 6.20: *Simultaneous fit of the 4 pA opposite-sign mass distributions in the mass range 1.3< M <2.0 GeV/c^2 and 4.5<M<8.0 GeV/c^2.*

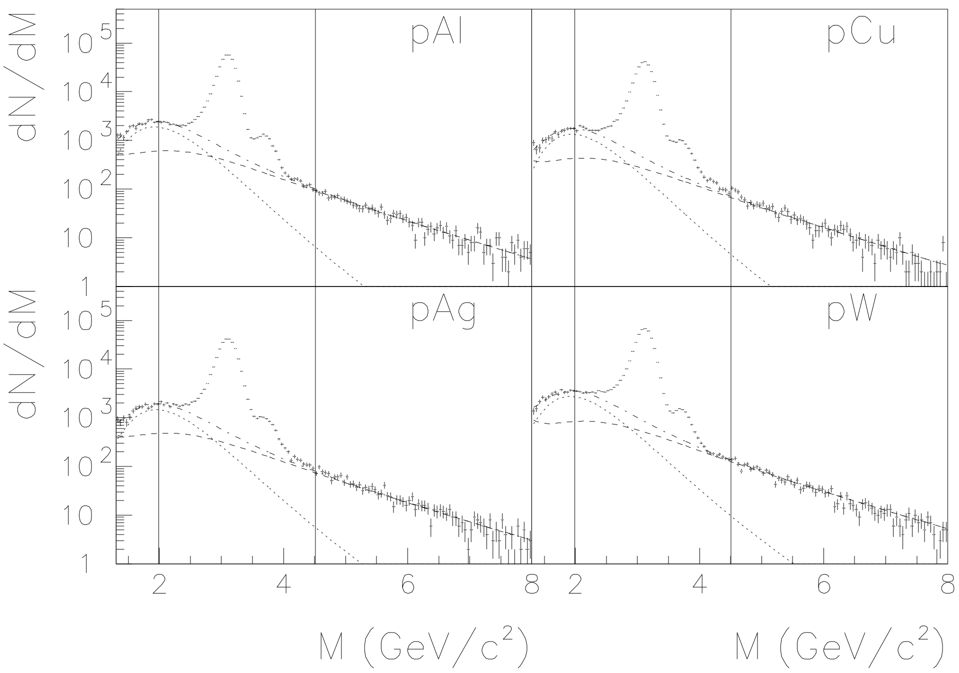

Figure 6.21: *Signal mass distributions compared with the curves resulting from the fit of the opposite-sign distributions shown in the previous figure, after background subtraction.*

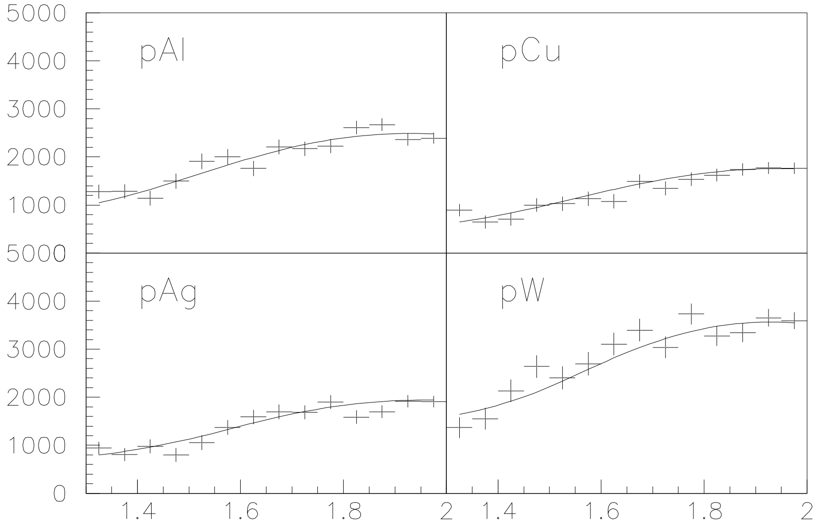

Figure 6.22: *Signal mass distributions compared with the curves resulting from the fit of the opposite-sign distributions shown in the previous figure, after background subtraction. The IMR is shown.*

a very good description of the pA mass distributions has also been achieved using the PYTHIA generated shapes with σ_{k_T}=0.9 GeV/c. In the following it is shown that the same nice agreement is found when the p_T, $cos\theta$ and y differential distributions for the pA systems are compared in the IMR region to the PYTHIA generated shapes normalised as in eq.6.6.

In fig.6.23 the pAl Monte-Carlo p_T, $cos\theta$ and y differential distributions are compared with the corresponding experimental distributions in the IMR; the Monte-Carlo distributions have been normalised as from eq.6.6 and have been generated with σ_{k_T}=0.9 GeV/c. The simulated curves well reproduce the experimental distributions with the exception of the large p_T region in the p_T spectrum. However, the PYTHIA event generator is based on leading order QCD calculations; if higher order corrections were taken into account a better data reproduction could be probably achieved. This different behaviour at large p_T was not visible on the PbPb and SU p_T differential distributions because of the lack of statistics for p_T >4 GeV/c.

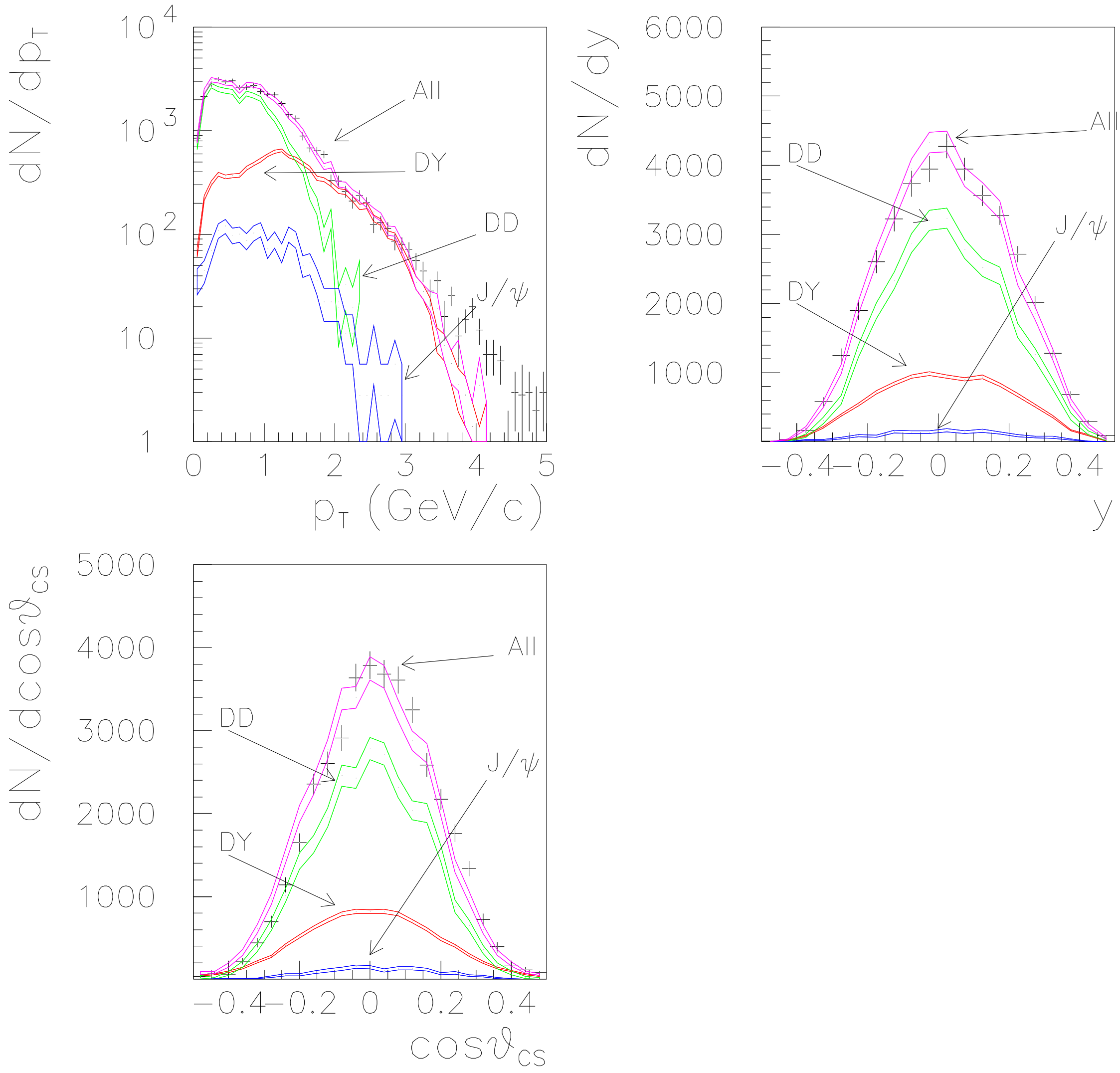

Figure 6.23: *pAl p_T, cosθ and rapidity differential distributions compared with the normalised PYTHIA generated distributions for σ_{k_T} = 0.9 GeV/c and* $1.5 < M < 2.5$ *GeV/c^2.*

6.9 Comparison with other methods

In the analysis of the SU and PbPb IMR presented at QM'96[2], the combinatorial background contribution to the IMR was fixed assuming that the multiplicity of secondaries in the peripheral S-U and Pb-Pb collisions is so large that charge correlation effects can be neglected. In this hypothesis the R_{BCK} factors were all set to 1.0. Even if we know that this approach is not correct, it can be instructive to perform the fit of the SU and PbPb mass spectra in the same hypothesis. In tab.6.6 the $D\overline{D}/DY$ ratios obtained when R_{BCK} =1.0 for all the PbPb E_T bins (1), is compared with the previously obtained values (0). The $D\overline{D}/DY$ values obtained in the two different approaches differ by $\simeq$ 20% in the more peripheral bins where the difference in the used R_{BCK} is $\leq$ 3%. The $D\overline{D}$ contribution in the more central collisions is enhanced by a factor of $\simeq$ 1.4 with respect with the one corresponding to the second E_T bin, a factor $\simeq$ 20% lower than the previously found enhancement. As expected, the use of our Monte-Carlo R_{BCK} factors leads to a more dramatic increase of the $D\overline{D}/DY$ values as a function of centrality, as shown in fig.6.24.

In tab.6.7 the same is listed for the SU system. The discrepancy between the two sets of values is $\simeq$10% in the more peripheral bins; the $D\overline{D}/DY$ enhancement amounts to 1.2, a factor $\simeq$ 8% lower than the previously measured enhancement. The larger sensitivity of the PbPb $D\overline{D}/DY$ values with respect to the two different sets of R_{BCK} is due to the larger contribution of the combinatorial background to the PbPb IMR mass spectra.

It is therefore mandatory to use the appropriate R_{BCK} values when dealing with systems where the combinatorial background strongly contributes to the IMR.

E_T bin	$\frac{D\overline{D}}{DY}\|_0$	$\frac{D\overline{D}}{DY}\|_1$
1	2.46 ± 0.32	3.20 ± 0.37
2	2.01 ± 0.23	2.52 ± 0.26
3	2.01 ± 0.22	2.41 ± 0.24
4	2.10 ± 0.22	2.40 ± 0.23
5	3.15 ± 0.29	3.35 ± 0.31
6	3.27 ± 0.31	3.35 ± 0.32
7	2.66 ± 0.27	2.74 ± 0.27
8	3.46 ± 0.36	3.46 ± 0.36
9	3.68 ± 0.37	3.68 ± 0.37

Table 6.6: *$D\overline{D}/DY$ obtained in the fit of the 9 PbPb mass spectra in the mass range 1.5< M <7.0 GeV/c^2, when the Monte-Carlo R_{BCK} values are used (0) and when R_{BCK}=1.0 for all the E_T bins (1).*

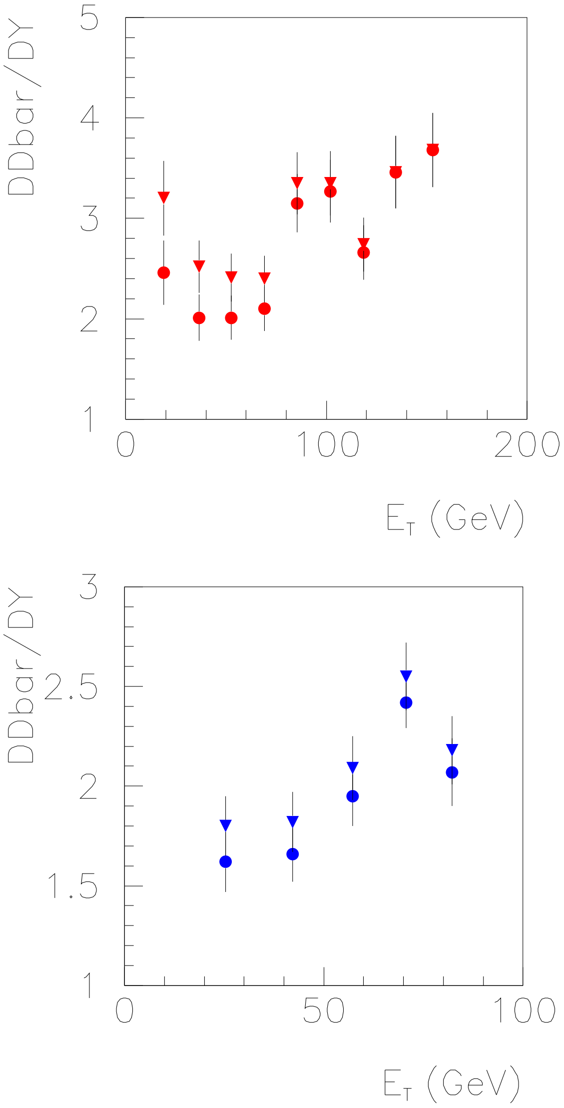

Figure 6.24: *The $D\overline{D}/DY$ ratios extracted from the analysis of the PbPb (top) and SU (bottom) systems is plotted vs. the transverse energy E_T. The values obtained when the Monte-Carlo R_{BCK} factors have been used (circles) are compared to the ones extracted when imposing R_{BCK}=1.0 for all E_T bins (triangles). No isospin correction has been applied.*

E_T bin	$\frac{D\overline{D}}{DY}\|_0$	$\frac{D\overline{D}}{DY}\|_1$
1	1.62 ± 0.15	1.80 ± 0.15
2	1.66 ± 0.14	1.82 ± 0.15
3	1.95 ± 0.15	2.09 ± 0.16
4	2.42 ± 0.13	2.55 ± 0.17
5	2.07 ± 0.17	2.18 ± 0.17

Table 6.7: *$D\overline{D}/DY$ obtained in the fits of the SU opposite-sign mass spectra when the Monte-Carlo R_{BCK} are used (0) and when R_{BCK}=1.000 for all the E_T bins (1).*

R_{BCK} free : PbPb and SU

It can be interesting to investigate if the shape of the mass differential distribution alone is able to determine the relative contributions of the different participating processes. We therefore fit the PbPb and SU mass spectra leaving the R_{BCK} as a free parameter in the fit. In fig.6.25 the different behaviour of the Monte-Carlo and free R_{BCK}'s is shown vs. the transverse energy E_T. The SU R_{BCK} free values are lower than the Monte-Carlo calculated ones, and vice-versa for the PbPb system. This is exactly the contrary of what we would expect, since charge correlation effects should decrease with increasing multiplicity, and the multiplicity of produced secondaries is linearly proportional to the transverse energy E_T. Furthermore, the SU free R_{BCK} factors are smaller than unity, and therefore lower than the value we expect when no charge correlation effect exists. The behaviour of the free PbPb R_{BCK} values well agree with the behaviour of our Monte-Carlo values, and the discrepancy between the two sets of values is not as large as for the SU system. On the other hand, the resulting $D\overline{D}/DY$ values differ by $\simeq 30\div50\%$ from the ones previously listed. As usual, even a small difference in the R_{BCK} value leads to large discrepancy on the extracted $D\overline{D}/DY$'s. This is again due to the larger contribution of the combinatorial background to the PbPb IMR.

We therefore conclude that the shape of the mass differential distribution alone can not give a reliable description of the IMR, and the Monte-Carlo R_{BCK} should be used to fix the combinatorial background contribution.

R_{BCK} free : pA

The $D\overline{D}/DY$ value quoted in eq.6.11 is affected by a very small statistical incertitude, much smaller than the incertitude associated with the SU and PbPb $D\overline{D}/DY$ ratios. The corresponding shape of the mass spectra in the IMR is better defined and here again we can investigate if the mass distribution alone can determine the relative importance of the $D\overline{D}$ and combinatorial background contributions. Since in the fit of the restricted mass range the number of free parameters is small, the

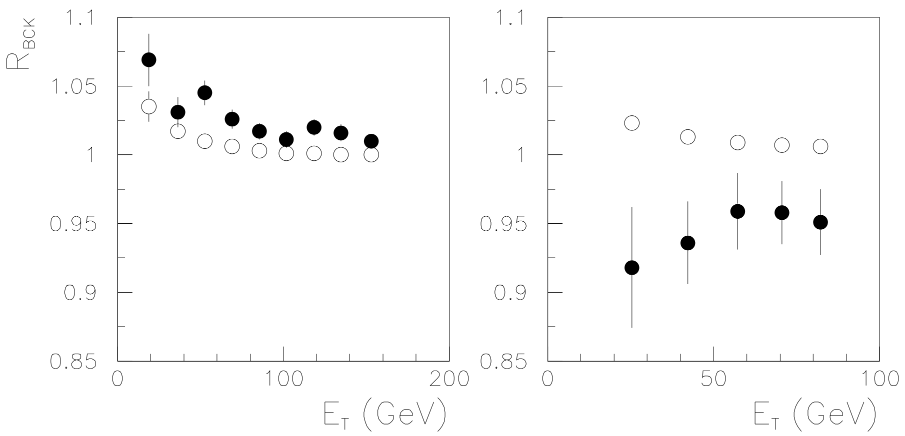

Figure 6.25: *R_{BCK} behaviour vs. E_T for the PbPb (left) and SU (right) systems: R_{BCK} free (filled circles) and Monte-Carlo R_{BCK} values (empty circles).*

total number of free parameters is still reasonable if the 4 R_{bck} factors are also left free. In fig.6.26 the result of the fit is shown on the signal mass spectra and in the IMR only. We find

$$\frac{D\overline{D}}{DY} = 4.22 \pm 0.13 \ (\chi^2{=}1.5) \tag{6.12}$$

which is in very good agreement with all the previous values. In tab.6.8 the found R_{bck} values are compared with the Monte-Carlo ones and the two sets of values very nicely agree. This impressive agreement is due to the limited number of degree of freedom allowed in the simultaneous fit of the pA mass spectra, where a common $D\overline{D}/DY$ has been imposed. If the pA data had been analysed one by one, leaving the R_{BCK} value as a free parameter in the fit, the R_{BCK} values would have been larger by a factor ≤ 10 %.

We have seen that the analysis of the pA data is stable against changes in the method used to perform the fit of the mass spectra, and that the shape of the mass spectra alone is able to determine the normalisations of the different processes contributing in the IMR. Thereafter, the discrepancy between the value in eq.6.12 and the value quoted in eq.6.10, which have both been obtained when fitting the restricted mass range, can be considered as an evaluation of the systematic error due to the method used for the combinatorial background subtraction. This discrepancy being very small, $\simeq 3\%$, it will be neglected in what follows.

6.10 Conclusion

In the present chapter we have shown that the SU and PbPb mass differential distributions can be well described as a superposition of dimuons from the DY process

$R_{BCK}\|_0$	$R_{BCK}\|_f$
1.06 ± 0.02	1.069 ± 0.005
1.06 ± 0.02	1.051 ± 0.005
1.06 ± 0.01	1.053 ± 0.005
1.05 ± 0.01	1.058 ± 0.003

Table 6.8: *The Monte-Carlo nominal R_{BCK} values (0) are compared with the ones obtained when simultaneously fitting the 4 pA systems in the mass range 1.3< M <2.0 and 4.5< M <8.0 GeV/c^2 whilst leaving the R_{BCK} factors as free parameters in the fit (f).*

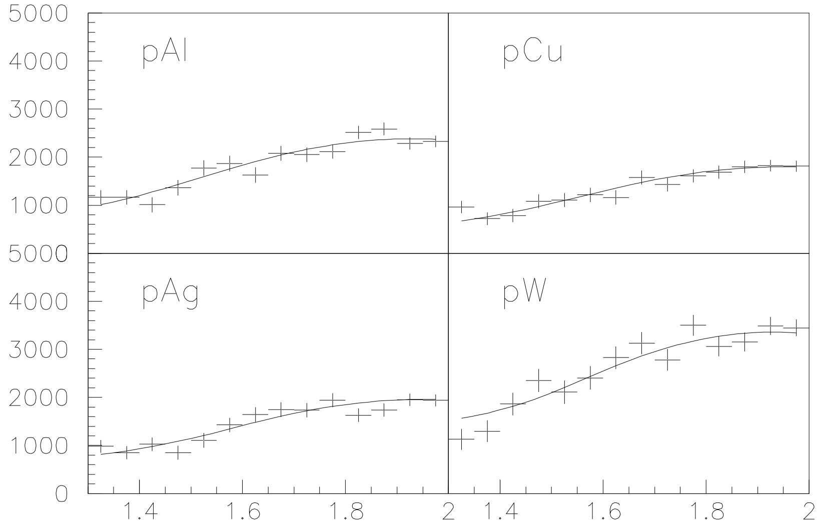

Figure 6.26: *Fit of the pA data in the restricted mass range 1.3 < M < 2.0 and 4.5< M <8.0 GeV/c^2. The PYTHIA generated Monte-Carlo shapes, with σ_{k_T} = 0.9 GeV/c, have been used. The Monte-Carlo R_{BCK} have been left as free parameters in the fit. Only the IMR is shown.*

and from the decay of charmed hadron pairs, after background subtraction. The latter has been performed using the R_{BCK} factors calculated in chapter 5. The systematic error associated with the method adopted for the combinatorial background subtraction has been found to be very small, ≃3%, and it is therefore always neglected in what follows.

We find that the $D\overline{D}/DY$ ratios extracted from the fit of the PbPb and SU mass spectra increase with the system size and the collision centrality. In order to support the hypothesis that the found excess is due to an enhanced open charm production, the p_T, cosθ and y differential distributions have been compared with the PYTHIA generated shapes, normalised as from the fit of the mass spectra with the inclusion of the enhanced charm component. With no additional hypothesis, a nice description of all the studied distributions has been obtained.

The pA systems have then been studied in order to determine the $D\overline{D}/DY$ pA reference value corresponding to no excess in the IMR. Again, the p_T, cosθ and y differential distributions have been compared with the PYTHIA shapes as above explained, obtaining a very good description of all the studied experimental distributions.

In the last section, the results of the present work have been compared with the results we would have got if the previous NA38/NA50 approach had been used as far as the R_{BCK} factor is concerned. If we imposed R_{BCK}=1.0 for all E_T bins, the steep increase with centrality of the $D\overline{D}/DY$ obtained for the PbPb system would have been smeared out, as shown in fig.6.24.

Finally, the option of leaving the R_{BCK} as a free parameter in the fit is shown to generally lead to a wrong estimation of the excess; only when the number of free parameters in the fit is small and the imposed constraints are extremely strong, as when studying the four pA systems in a simultaneous way, the shape of the mass differential distribution alone can be able to correctly determine the normalisation parameters of the contributing processes.

Bibliography

[1] Amir Bohrani, PhD thesis, April 1996, Uni. Paris 6.

[2] E.Scomparin, for the NA50 Collaboration, at the Quark Matter '96 Conference, Heidelberg, Germany (1996)

[3] PDFLIB 7.09, Users's Manual, CERN/PPE (1997)